*Indian J. Phys.* **82 (12)** 1655-1664 (2008)

IJP

# Heliographic distribution of X-ray solar flares and their association with geomagnetic disturbances in relation to solar radio emissions and coronal mass ejections

A P Mishra*, V K Mishra, Roopali Tripathi and B N Mishra
Department of Physics, Awadhesh Pratap Singh University, Rewa-486 003 Madhya Pradesh, India

E mail apm_apsu@yahoo co in

*Received 6 March 2008, accepted 29 May 2008*

**Abstract** : Solar X-ray flares are the tremendous spectacular explosions on the surface of the sun Major X-ray flares (M and X class) have been selected to study their heliographic distributions during solar cycle 23 The occurrence of geomagnetic storms (Dst magnitude $\leq -100$ nT) associated with X-ray flares, coronal mass ejections (CMEs) and solar radio emissions (SREs) has also been analyzed for the period 1996 to 2006 Though, the occurrence of X-ray flares (Type-M and Type-X) is equally distributed in the entire solar regions, however, the X-ray flares originated from northern/western hemisphere of the sun have been found more effective in producing major geomagnetic storms as compared to southern/eastern hemisphere Out of 78 geomagnetic storms, 86% are found to be associated with halo (central position angles $\approx 360°$) and partial halo (central position angles $\geq 120°$) CMEs and about 40% geomagnetic storms are associated with sudden storm commencement (SSC) The observed geomagnetic storms have also been found to be associated with type II (71%) and type IV (54%) solar radio bursts The results are discussed in the light of earlier findings

**Keywords** : X-Ray solar flares, coronal mass ejections, solar radio emissions, geomagnetic storms

**PACS Nos.** : 96 60 -j, 96.60 Q-

## 1. Introduction

Solar X-ray flare is a violent explosion and spectacular short-lived phenomenon that occur in the sun's outer atmosphere. The solar outputs in terms of particles and field ejected out into interplanetary medium influences the geomagnetic conditions. Sometimes, the X-ray solar flares of lower importance are also able to produce geomagnetic storms. X-Ray flares are classified as type B ($I < 10$), C($10^{-6} \leq I < 10^{-5}$), M ($10^{-5} \leq I < 10^{-4}$) and X ($10^{-4} < I$) according to the peak flux (I) measured in watt per square meter ($w/m^2$) of 100 to 800 pico meter near earth.

Geomagnetic storms are large disturbances in the magnetic field of the earth

*Corresponding Author

persisting for several days or more. The geo-space environment is dominated by geomagnetic disturbances originating from the sun *via* interplanetary medium, such as solar flares, X-ray flares, CMEs, SREs, planetary index Ap, interplanetary magnetic field (IMF) and their southward component (Bz), which are responsible for large geomagnetic storms [1–3]. Coronal mass ejections (vast structure of plasma and magnetic fields) expelled from the sun are now known to be a main cause for major interplanetary disturbances and geomagnetic storms.

The main solar and interplanetary cause of geomagnetic storms has been established for decades. The exact solar sources and their characteristics were not well established until the advent of Solar and Heliospheric Observatory (SOHO) mission [4]. When CMEs event occurs, they compress and push the ambient solar wind plasma and magnetic field line. The distribution of flares on the solar disk shows strong north-south asymmetry for all classes of flares. From the N-S distribution of soft X-ray flares ($\geq$ M1) during solar cycle 20 to 21, it was concluded that the spatial distribution of flares varies within a solar cycle such that the preponderance of flares occurs in the north during the early part of the cycle and then moves south as the cycle progress [5–7]. Recently, the northern hemisphere has been reported to be dominant in general during the rising phase of the cycle 23. The dominance of northern hemisphere shifted towards the solar maximum [8]. It has also been estimated that Halo CMEs are the main cause of geomagnetic disturbances [9–11]. It is also reported that the number of strong flares reach their maximum in the year of maximum solar activity [12]. The effect of CMEs on earth magnetosphere has been extensively studied, which lead to conclude that interplanetary shocks, large solar particle events and non-recurrent geomagnetic storms are caused by CMEs [11,13,14].

In the present paper, an attempt has been made to study the heliographic distribution of X-ray solar flares and association of geomagnetic disturbances with X-ray flares, SREs and CMEs. The aim of this paper is to find out the active regions of the solar disk, which are responsible to produce major geomagnetic storms during solar cycle 23. The dominance of X-class flares occurring in different quadrants has also been investigated during 1996 to 2006, which is more effective in producing storms.

## 2. Data analysis

In the present study, we have analyzed the heliographic distribution of X-ray solar flares and their association with geomagnetic disturbances in relation to solar radio emissions and coronal mass ejections. Here we have sorted out the X-ray solar flares (Type-M and Type-X) during the period 1996 to 2006. The spatial distribution of X-ray flares has been analyzed with respect to heliographic latitude and longitude in the interval of 10°. To study the effect of different form of solar activity on geomagnetic field, here we have selected large geomagnetic storms which possess disturbed storm time index (Dst) decreases of less than −100 nT, during the period 1996-2006. The disturbance storm time index is the conventional measure of ring current intensity and energy observed

at earth's surface over low and moderate latitudes It is the best indicator of ring current intensity and a very sensitive index to represent the degree of solar disturbances The Dst index gives the strength of the average depression of the earth's magnetic field at the equator and is commonly used to measure of the strength of magnetic storms To see the association of Dst with X-ray flares, SREs and/or CMEs possible time lags of 1 to 4 days (Travel time depending on the solar wind plasma velocity from source region to interplanetary region near earth) have been considered Furthermore, for the present study, we have also considered the type II and IV radio bursts associated with geomagnetic storms Most of the data *e g* (Dst), X-ray flare data and radio burst data has been obtained from the Solar Geophysical Data (Prompt and Comprehensive Report of U S Department of Commerce, NOAA, USA) monthly issues, whereas the occurrence of CMEs is obtained from the website http //cdaw gsfc nasa gov/cme_list

## 3. Results and discussion

Solar active regions are identified by the location of different class of major flares, which eject vast amount of energy and matter from solar atmosphere and affect the cosmic ray intensity and geomagnetic field [15] A solar flare produces copious radiations across the full electromagnetic spectrum The X-ray flares have higher energy and greater penetrating power The variation of annual mean of the sunspot number with type-X ($I > 10^{-4}$ w/m$^2$) and type-M ($10^{-5} \leq I \leq 10^{-4}$ w/m$^2$) flares are shown in Figure 1. This figure shows that minimum number of type-X and M-class flares have occurred in the year 1996 whereas the occurrence is maximum in the year 2001 for both type of flares From which, it is clear that the occurrence of type-X and M-class

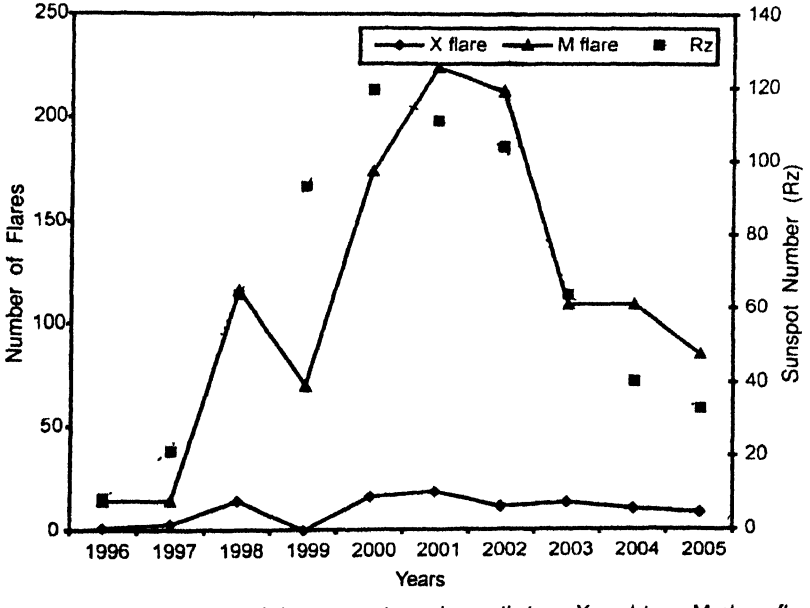


**Figure 1.** The variation of annual mean of the sunspot number with type-X and type-M class flares

flares follows the phase of solar cycle. Further the cross-plot between X-class flare and sunspot number shows high degree of correlation between them (Correlation coefficient $r \approx 0.84$).

The distribution of X-ray solar flares (Type-M and Type-X) around the solar disk during the period 1996-2006 is shown in Table 1. The distribution shows that the

**Table 1.**

X-Flare distrubution (M-type)

| | 0–10 | 10–20 | 20–30 | 30–40 | 40–50 | 50–60 | 60–70 | 70–80 | 80–90 | 90–100 | Total |
|---|---|---|---|---|---|---|---|---|---|---|---|
| N | 105 | 275 | 106 | 10 | 2 | 0 | 0 | 0 | 0 | 0 | 498 |
| S | 81 | 295 | 114 | 10 | 0 | 0 | 0 | 0 | 0 | 0 | 500 |
| E | 54 | 70 | 76 | 49 | 60 | 59 | 55 | 41 | 18 | 7 | 489 |
| W | 51 | 42 | 54 | 69 | 61 | 55 | 73 | 52 | 34 | 18 | 509 |
| Total | 998 | | | | | | | | | | |

X-Flare distrubution (X-type)

| | 0–10 | 10–20 | 20–30 | 30–40 | 40–50 | 50–60 | 60–70 | 70–80 | 80–90 | 90–100 | Total |
|---|---|---|---|---|---|---|---|---|---|---|---|
| N | 7 | 24 | 8 | 4 | 0 | 0 | 0 | 0 | 0 | 0 | 43 |
| S | 4 | 30 | 10 | 1 | 0 | 0 | 0 | 0 | 0 | 0 | 45 |
| E | 4 | 1 | 2 | 5 | 4 | 2 | 5 | 3 | 7 | 0 | 33 |
| W | 5 | 12 | 4 | 6 | 5 | 6 | 4 | 1 | 9 | 3 | 55 |
| Total | 88 | | | | | | | | | | |

number of X-ray flares have almost uniformly occurred over the entire solar disk whereas, the occurrence of major solar flares (Imp $\geq$ 1B) is more in northern/western hemisphere as compared to southern/eastern hemisphere [14]. It is also evident from this table that most of the X-ray flares of type-M are produced in the range 0–40° latitude, which holds good for both northern and southern hemisphere. No X-ray flares have occurred beyond 50° in northern or southern hemisphere. Moreover, the longitudinal distribution of X-ray flares (Type-M and Type-X) has been found to occur equally throughout the entire solar region. The occurrence of geomagnetic storms (Dst magnitude –100 nT) and their association with solar processes is shown in Table 2. It appears from the table that the coronal mass ejections and solar radio emissions are the main causes to produce major geomagnetic disturbances. Out of selected 78 large geomagnetic storms, 83% geomagnetic storms are associated with coronal mass ejections (halo CMEs and partial halo CMEs), which are in conformity with the results reported earlier [9–11].

Geomagnetic storms are a major indicator of disturbance in the earth's magnetosphere that occur when the interplanetary magnetic field (IMF) turns southward and remain so for a prolonged period [16,17]. Soon, after knowledge about coronal mass ejections (CMEs), it was found that major geomagnetic storms are highly correlated with the CMEs [18,19]. Reconnection between the southward-directed component of the interplanetary magnetic field (Bz), and the northward directed

**Table 2.** Association of geomagnetic storms with the solar parameters

| Events (Out of 78) | Percent |
|---|---|
| Dst +Type II SRE(without Type IV) | 22% (17 out of 78) |
| Dst + Type II SRE (Total Type II) | 71% (55 out of 78) |
| Dst + Type IV SRE (without Type II) | 4% (3 out of 78) |
| Dst + Type IV SRE (Total Type II) | 54% (42 out of 78) |
| Dst + CME + Flare (Only) | 4% (3 out of 78) |
| Dst + CME + SRE (Only) | 32% (25 out of 78) |
| Dst + CME + SRE + Flare | 40% (31out of 78) |
| Dst + SRE + Flare | 5% (4 out of 78) |
| Dst + CME | 10% (9 out of 78) |
| Dst + SRE | 5% (4out of 78) |
| Dst + SSC | 40% (32 out of 78) |
| Dst + Flare | No event (0 out of 78) |

geomagnetic field occurs at the dayside magnetopause and this reconnection transports energy from the solar wind into the magnetosphere. During a storm, the enhanced ring current is created and it greatly influences the structure of magnetospheric regions, which, in turn, results in a significant electric potential on conductors in all kinds of operating systems. As more advanced and interconnected systems are employed, the effect of the upper atmosphere becomes more profound. The impact of the interplanetary shocks on the outer part of the magnetosphere of the earth change the geomagnetic field component (H) suddenly and known as sudden storm commencement. Eventatuly, a new steady electric current is stabilized throughout the magnetopause and hydro magnetic waves are genetared. When this wave reaches the earth surface through the ionosphere, produces sudden storm commencement (SSC). CMEs originating from close to the disk center (most of which become front-side halos) directly impact Earth and produce geomagnetic storms provided their magnetic field has a prominent

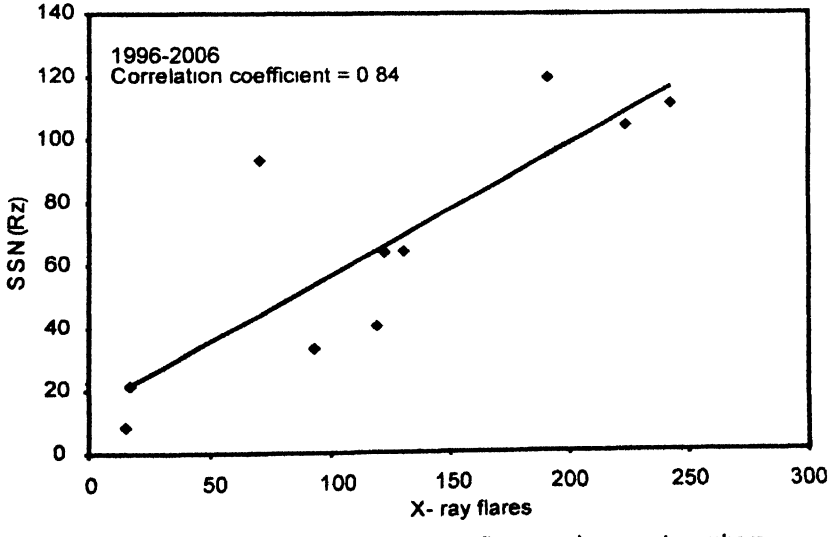


**Figure 2.** Cross-plot between X-ray flares and sunspot numbers

southward component (Bz). The impact is marked by the sudden commencement if the CME drives a shock. Interplanetary coronal mass ejections (ICMEs) with a flux rope structure (magnetic cloud), almost always cause a storm because either the front or the rear section of the ICME contains effective Bz component. Occasionally CMEs arrive at Earth with a high inclination resulting in an intense storm (when the magnetic field is fully southward) or no storm at all (when the magnetic field is fully northward) The 40% geomagnetic storms occurred during the cycle 23 are associated with SSC

A distribution of X-ray flares (Type-M and Type-X) associated with geomagnetic storms (Dst $\leq -100$ nT) during the said period is shown in Figures 3(a,b) and 4(a,b)

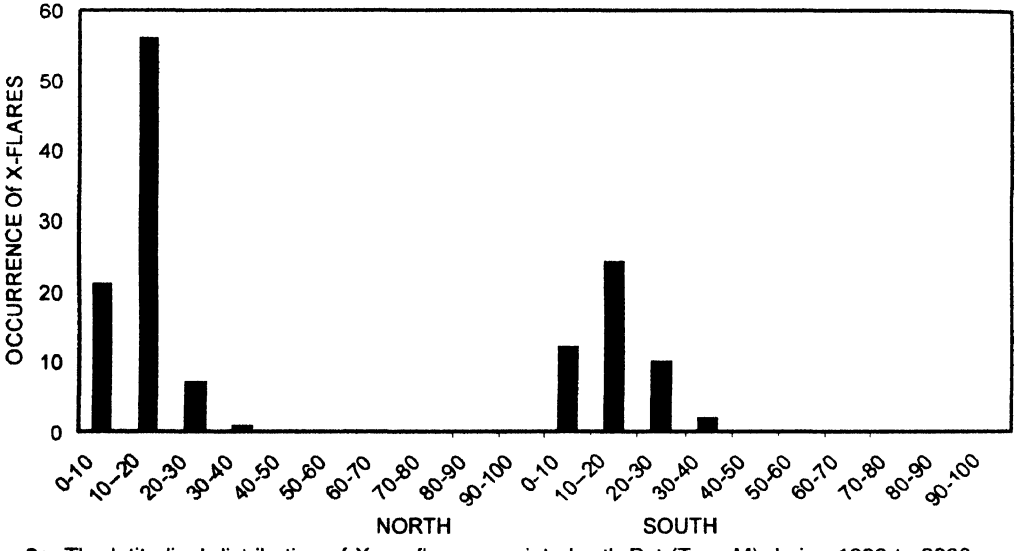


**Figure 3a.** The latitudinal distribution of X-ray flare associated with Dst (Type-M) during 1996 to 2006.

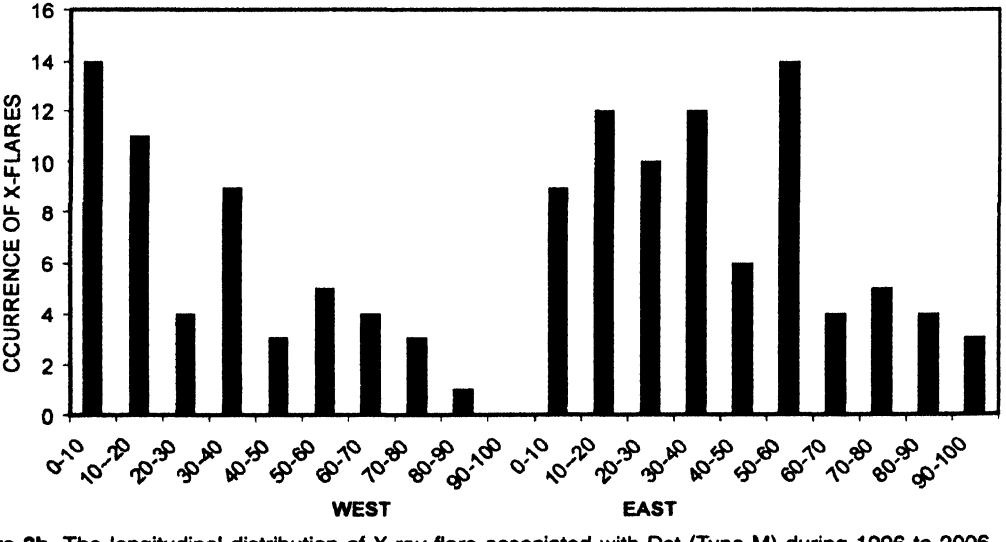


**Figure 3b.** The longitudinal distribution of X-ray flare associated with Dst (Type-M) during 1996 to 2006.

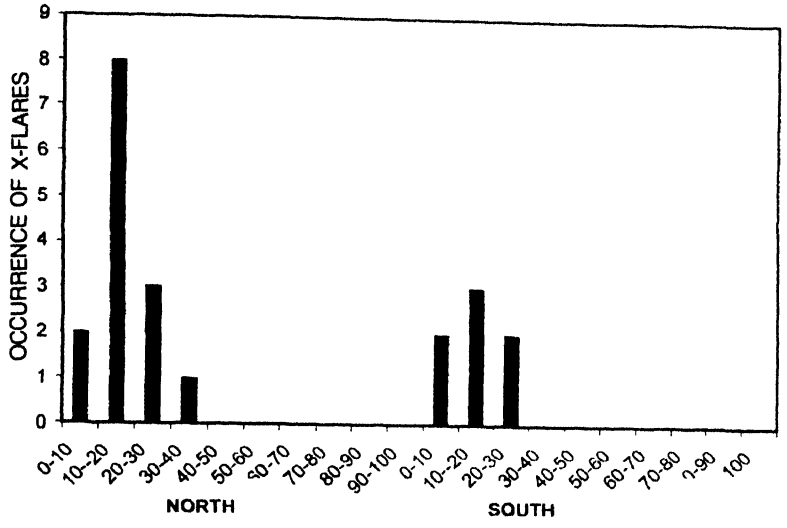


**Figure 4a.** The latitudinal distribution of X-ray flare associated with Dst (Type-X) during 1996 to 2006

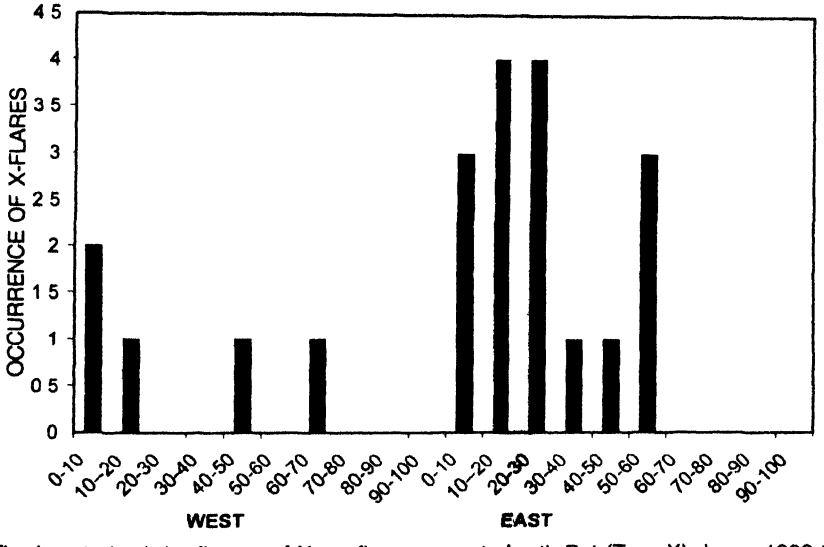


**Figure 4b.** The longitudinal distribution of X-ray flare associated with Dst (Type-X) during 1996 to 2006.

From these figures, it is clear that the X-ray flare (Type-M and Type-X) occurred in northern/western hemisphere is more effective in producing large geomagnetic storms as compared to southern/eastern hemisphere. It is also evident that only those X-ray flares of type-M are more effective in producing geomagnetic storms, which have occurred in 0–40° of longitudinal and latitudinal regions. The X-class flares occurring within 0–40° N-S hemispheres are more effective in producing large geomagnetic storms, whereas, in E-W hemisphere only those X-class flares are effective which occur within the range 0–20°. The heliographic distributions of X-ray flares responsible for geomagnetic storms (Type-M and Type-X) in quadrants area of the solar disk are

depicted in Figures 5(a,b). These figures show that the majority of X-ray flares (Type-M and Type-X) occurred in north-west region are responsible for producing major geomagnetic storms during solar cycle 23. The most frequently observed solar phenomenon at meter and decimeter wavelengths consists of long series of burst called storm bursts and the radiation of such type is called the noise storm or enhanced radiation [20]. The solar active region produces different types of bursts in radio range The major solar flares are frequently accompanied by out bursts at meter wavelengths lasting from 5–30 minutes and are termed as type II radio bursts. The emissions covering all wavelengths from microwaves to tens of meter range and lasting an hour or so are known as type IV radio bursts. These bursts are connected with emissions of plasma from deep atmosphere of the sun [9,21] and hence are well correlated with CMEs and geomagnetic storms.

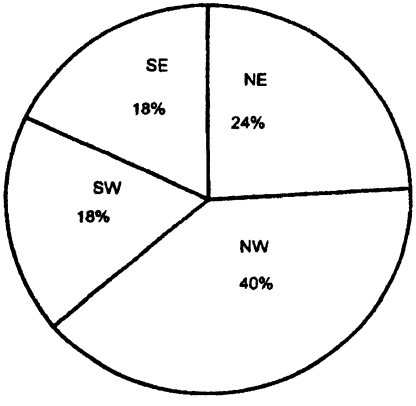


**Figure 5a.** The quadrant distribution of X-ray flares (Type-M) associated with major geomagnetic storms.

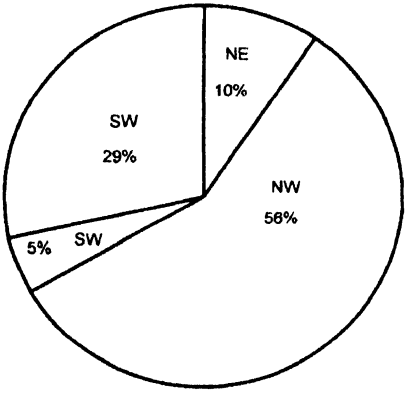


**Figure 5b.** The quadrant distribution of X-ray flares (Type-X) associated with major geomagnetic storms

## 4. Conclusions

Based on the observational results discussed above, the following conclusions are drawn :

(i) Although, the occurrence of X-ray flares (Type-M and Type-X) is found to be almost equally distributed over the entire solar cycle, however, the X-ray flares occurred in northern/western hemisphere is found more effective in producing geomagnetic disturbances as compared to southern/eastern hemisphere on the solar disk.

(ii) 46% geomagnetic storms are found to be associated with X-ray flares and 86% storms with halo/partial halo CMEs.

(iii) The X-ray flares of type-M are more responsible as compared to type-X for producing geomagnetic storms; moreover, the X-class flares occurring in north-west region are more effective in producing geomagnetic storms.

(iv) The observed geomagnetic storms have also been found to be associated with type II (71%) and type IV (54%) solar radio bursts and 40% with sudden storm commencement

(v) 10% geomagnetic storms are found to be associated with only halo/partial halo CMEs and 5% with solar radio emissions only

**Acknowledgments**

This work is supported by the Indian Space Research Organization (ISRO), Bangalore (India) under the RESPOND Programme The authors thankfully acknowledge the ISRO for providing the research grant The data used here has been taken from the SOHO/ LASCO coronagraphs which enable to observe CMEs with unprecedented continuity and spatial coverage and hence we could have a better picture of the whole phenomenon from minimum to maximum phase of the solar cycle 23 We gratefully acknowledge all the members of the LASCO consortium (Naval Research Laboratory, USA, University of Birmingham, UK, Laboratoire d'Astronomie Spatiale, France and Max-Plank-Institute for Aeronomie, Germany) who built the coronagraphs and acquired the data used in this work

The author thanks the anonymous referees for their valuable comments for the improvement of this paper

**References**

[1] I Sabbah *J Geophys Res Lett* **27** 13 (2000)

[2] W D Gonzalez, J A Joselyn, Y Kamide, H W Kroehl, G Rostoker, B J Tsurutani and V M Vasyliunas *J Geophys Res* **99** 5771 (1994)

[3] G Zhang and L F Burlaga *J Geophys Res* **93** 2511 (1988)

[4] G E Brueckner R A Howard M J Koomen, C M Korendyke, D J Michels J D Moses, D G Socker, K P Dere, P L Lamy, A Llebaria, M V Bout R Schwenn G M Simnett, Bedford D K and C J Eyles *Solar Physics* **162** 357 (1995)

[5] R K Mitra, S K Sarkar and M K Gupta *Indian J Radio and Space Physics* **1** 170 (1972)

[6] H A Garcia and M Dryer *Solar Physics* **109** 119 (1987)

[7] A P Mishra, B N Mishra, M Gupta and V K Mishra *Indian J Radio and Space Physics* **37** 237 (2008)

[8] B Joshi, P Pant and P K Manoharan *J Astrophy Astro* **27** 151 (2006)

[9] J T Gosling, D J Mc Comes, J L Phillips and S J Bame *J Geophys Res* **96** 7831(1991)

[10] S W Kahler *Anne Rev Astron Astrophys* **30** 113 (1992)

[11] R Tripathi and A P Mishra *Proc 29th Int Cosmic Ray Conf* (Pune) **1** 161 (2005)

[12] S C Dubey and A P Mishra *Current Science* **78** 11 (2000)

[13] K Kai, D B Melrose and S Suzuki *Solar Radio Physics* **415-441** (1985)

[14] A P Mishra, B N Mishra, M Gupta and V K Mishra *Int Conf on Challenges for Solar Cycle-24, held at PRL Ahmedabad, Jan 22-25, Abstract Book 85*

[15] A P Mishra, M Gupta and V K Mishra *Solar Physics* **239** 475 (2006)

[16] G Rostoker and C G Falthammar *J Geophys Res* **72** 5853 (1967)

[17] C T Russell, R L McPherron and R K Burton *J Geophys Res* **79** 1105 (1974)

[18] L F Burlaga, E Sittler, F Mariani and R Schwenn *J. Geophys. Res.* **86** 6673 (1981)

[19] R M Wilson and E Hildner *Solar Physics* **91** 169 (1984)

[20] N R Sheeley, R A Howard, D J Michels, R D Robinson, M J Koomen and R T Stewart *Astrophysical J. Part I* **279** 839 (1984)

[21] E Zlotnik, V V Ya Zaitsev, H Aurass, G Mann and A Hofmann *Astronomy & Astrophys* **410** 1011 (2003)

*Indian J. Phys.* **82 (12)** 1665-1669 (2008)

IJP

# An evaluation of plasmon frequency associated with charge carriers for heavy electron systems

Prajwalit Shikha[1]*, V K Sinha[2] and J D Dubey[1]

[1]Department of Physics, Vinobha Bhave University, Hazaribag-825 301, Jharkhand, India

[2]Department of Physics, St. Columba's College, Hazaribag-825 301, Jharkhand, India

E-mail prajwalitshikha@yahoo.co.in

*Received 27 February 2008, accepted 29 September 2008*

**Abstracts :** We present an evaluation of the plasmon frequency associated with charge carriers of heavy electron systems using the theoretical model of Millis, Lavagna and Lee. For such systems, there are two types of plasmon frequencies – one is related with the uncorrelated conduction electrons which gives high plasmon frequency, and the other is low plasmon frequency which depends upon the Fermi temperature $T_f$ and the total carrier density $n$ which is the sum of the carrier densities $n_c$ and $n_f$ due to conduction and $f$-electrons respectively.

**Keyowrds :** Plasmon frequency, uncorrelated conduction electrons, Fermi temperature, heavy electron systems.

**PACS Nos. :** 71.27.+a, 71.45.Gm, 72.30.+q, 73.50.Mx

## 1. Introduction

Heavy electron systems are electrically conducting materials with peculiar low temperature properties that distinguish them from ordinary metals [1,2].

In these systems there are two types of electrons :

(i) Conduction electrons whose role is dominant below Fermi temperature $T_F$;

(ii) $f$-electrons whose role is dominant above $T_F$.

At high temperature, these systems behave as a weakly interacting collection of $f$-electron moments and conduction electrons with quite ordinary masses. At low temperatures, the $f$-electron moments become strongly coupled to the conduction electrons and to one another, and the conduction electron effective mass ($m^*$) is 10 to 100 times larger the bare electron mass ($m$). The enhancement of the effective mass

*Corresponding Author

can be assigned to the presence of localized *f* electrons in all heavy electron systems. These may be Ce ions with 4*f* electrons or U or Np ions with 5*f* electrons. Prominent examples are $CeAl_3$, $CeCu_2Si_2$, $CeCu_6$, $UBe_{13}$, $UPt_3$, $UCd_{11}$, $U_2Zn_{17}$ and $NpBe_{13}$. The 4*f* or 5*f* electrons interacting with the bands of the delocalized electrons (*d* or *s*) can be considered as the "heavy electron" [3,4] of these systems. For the electromagnetic response of heavy electron systems, the optical experiments and the analysis of the experimental data give the value of the scattering rate and the plasmon frequency associated with the charge carriers. For $CeAl_3$, Awasthi [5] have obtained the real part of optical conductivity $\sigma(\omega)$ [= $\sigma_1(\omega) + i\sigma_2(\omega)$] from Kramers-Kronig analysis of the excitation spectrum data.

In this paper, we report the evaluation of the plasmon frequency of various heavy electron systems. These systems possess two types of plasma frequency [6,7]. One is the high plasma frequency and is concerned with the uncorrelated conduction electrons. The other is the low plasma frequency and depends upon the Fermi temperature $T_F$ and the total carrier density $n$ (= $n_c + n_f$), where $n$ and $n_f$ are carrier densities due to conduction and *f* electrons respectively.

## 2. Method of calculation

We have used the theoretical formulation of Millis *et al* [6,7] which is based on a study of the low temperature properties of the lattice Anderson Hamiltonian, in the Kondo limit. It describes a band of nearly free electrons hybridizing with a very highly correlated band of electrons. In the absence of this hybridization, each *f* electron is confined to one lattice site localized orbitals which are far below the Fermi energy. This model is believed to contain the essential physics of heavy electron systems. It has a nonmagnetic ground state that behaves like a Fermi liquid with large effective mass.

For the evaluation of $\sigma(\omega, T)$, scattering must be taken into account. There are two possible sources of scattering of electrons in these systems. One is the scattering of electrons from the impurities and the other is the scattering from boson fluctuations. This latter turns out to be in some ways analogous to electron-phonon scattering. One can apply Matthiesen's rule [8] in which the resistivities due to different scattering mechanism are to be added. Thus, if in the presence of impurities only the conductivity is $\sigma_i$ and in the presence of boson only the conductivity is $\sigma_b$ then the total conductivity is given by

$$\sigma^{-1} = \sigma_i^{-1} + \sigma_b^{-1}. \tag{1}$$

Matthiessen's rule is believed to be valid when the various scattering mechanism are not momentum dependent and are weak.

At sufficiently low temperatures, only impurity-scattering is relevant. To compute the corresponding impurity component $\sigma_i(\omega, T)$ of $\sigma(\omega, T)$, the disorder must be coupled into the system. Millis and Lee [6] obtained

$$\sigma_1(\omega) = \left[ne^2/m_b\right] \left[\tau_1 / \left\{1 + (m^*/m_b)^2\, \omega^2 \tau_1^2\right\}\right]$$

$$= \left[ne^2/m^*\right] \left[\tau_1^* / \left\{1 + \left(\omega\tau_1^*\right)^2\right\}\right] \tag{2}$$

introducing the definition, $\tau_1^*/\tau_1 = m^*/m$.

Freytag and Keller [9] calculated the dynamical conductivity for heavy electron systems, taking into account the effect of impurity scattering within a mean field approximation of the Anderson Hamiltonian They obtained a dynamical conductivity characterized by a narrow low-frequency - Drude peak superimposed on a broad background with a minimum near $k_B T_K$ presumably due to a mixture of the broadened interband transition and the Drude behaviour of the conduction electrons Two characteristic plasma frequencies are then expected . the one at high frequency is given by

$$\omega_p^2 = 4\pi n_c e^2/m_b\,. \tag{3}$$

This identifies the uncorrected conduction electrons. The other is at low frequency and associated with the heavy plasmons, given by

$$\varpi_p^* = \sqrt{\left[6\,(1 + n_f/n_c)\right] \times T^*}\,, \tag{4}$$

where $T^*$ is the renormalized Fermi temperature (usually identified with $T_K$) and $n_c$ and $n_f$ are the carrier densities due to conduction and $f$ electrons respectively

To include the scattering from bosons ($\sigma_b$), application of Matthiessen's rule leads to the result that the conductivity is simply formed by adding the $c$-electron self-energy due to electron-boson interactions. Moreover, because the $f$ electrons are dispersionless in this approach, the applied model is not Galilean invariant. Keeping in mind that the umklapp process can occur at all nonzero temperatures and interpreting the imaginary part of the $c$-electron self-energy as a temperature and frequency-dependent scattering rate $1/2\pi\tau(\omega,T)$. Millis and Lee [6] found

$$1/\tau(\omega,T) = 1/\tau_1 + (m^*/Nm_b)\cdot(\omega^2 + \pi^2 T^2)/\varepsilon_f\,. \tag{5}$$

At $T = 0$, and for $\omega < \omega_c$, where

$$\omega_c^2 = N\varepsilon_f (m_b/m^*)/\tau_1, \tag{6}$$

the impurity scattering dominates and eq. (2) applies. For larger $\omega$, one finds

$$\sigma_1(\omega) \sim \sigma_b \sim (ne^2/m_b)\left(1/N(m^*\ \ m_b\right)\varepsilon_f \sim ne^2/m_b W\,. \tag{7}$$

Therefore for $\omega > \omega_c$ the conductivity becomes very small and approximately independent of frequency.

Now consider the case $T = 0$, and $\omega = 0$. The resistivity $\rho = \sigma^{-1}$ and after averaging eq. (5) over the energies of thermally excited electrons, one gets

$$\rho = \left(m_b/ne^2\right)\left(1/\tau + 4m^*\pi^2T^2/3Nm_b\varepsilon_f\right). \tag{8}$$

## 3. Results and discussion

We have calculated the plasma frequency of different heavy-electron-systems using the two relations given in eqs. (3) and (4), at the renormalized Fermi temperature $T^*$. The heavy electron plasmon mode reflects not only the heavy quasiparticle mass $(m^*/m)$ but also the renormalized Coulomb screening The other plasmon frequency is the unscreened heavy plasmon and is associated with the spectral weight functions and narrow Drude like behaviour of the conduction electrons. The results are given in Table 1 where the calculated ratio of the effective mass to ordinary mass of the electron in these heavy-electron-systems are also given.

**Table 1.** Plasmon frequency of different heavy electron systems

| Heavy electron systems | $m^*/m$ | $\omega_p^*$(eV) using eq (3) | $\omega_p^*$(eV) using eq (4) | $T^*$ (Kelvin) |
|---|---|---|---|---|
| $CeCu_2Si_2$ | 220 | 9 371 | 10 446 | 11 340 |
| $CeAl_3$ | 1620 | 3 453 | 4 204 | 4 564 |
| $CeCu_6$ | 1300 | 3 856 | 4 053 | 4 400 |
| $CePd_3$ | 370 | 6 412 | 7 559 | 8 210 |
| $UPt_3$ | 450 | 6 552 | 5 296 | 5 700 |
| $UBe_{13}$ | 1100 | 1 756 | 2 361 | 2 560 |
| $URu_2Si_2$ | 180 | 11 073 | 9 563 | 10 380 |
| $UCu_5$ | 250 | 8.790 | 7 344 | 7.974 |
| $U_2Zn_{17}$ | 500 | 6 216 | 6 519 | 7 07 |
| $UPd_2Al_3$ | 150 | 11 348 | 12 698 | 13 79 |

We have also studied the temperature dependence of resistivity $\rho(T)$ for two heavy-electron-systems $UPt_3$ and $CeAl_3$ and have been calculated using eq. (8), and are given in Table 2 from 5 to 300 K. The $CeAl_3$ compound has a hexagonal crystal structure and its resistivity displays $T^2$ dependence up to $T = 0.3$ K. Our calculation gives $\rho_0 = 0.95$ $\mu\Omega$ cm. The experimental value [10] is $\rho_0 = 0.76$ $\mu\Omega$ cm. The actinide $UPt_3$ also has a hexagonal structure and displays an anisotropic resistivity. The resistivity is different for *ab* plane and along the hexagonal *c* axis. It is also found to follow the $T^2$ behaviour. Our calculated results for $UPt_3$ for *c* axis are very much near to $[\rho(T)]_{exp}$ at *c*-axis.

**Table 2.** Temperature dependence of resistivity $\rho(T)$ for $UPt_3$ and $CeAl_3$

| $T$ (Kelvin) | $\rho(T)$ for $UPt_3$ ($\mu\Omega$ cm) | $\rho(T)$ for $CeAl_3$ ($\mu\Omega$ cm) | $T$ (Kelvin) | $\rho(T)$ for $UPt_3$ ($\mu\Omega$ cm) | $\rho(T)$ for $CeAl_3$ ($\mu\Omega$ cm) |
|---|---|---|---|---|---|
| 5 | 12 6 | 150 2 | 190 | 88 5 | 160 5 |
| 10 | 21 2 | 162 6 | 200 | 90 2 | 158 2 |
| 50 | 32 8 | 210 8 | 220 | 92 0 | 156 0 |
| 100 | 78 3 | 200 5 | 240 | 94 3 | 153 9 |
| 150 | 80 4 | 180 4 | 260 | 96 5 | 150 2 |
| 160 | 82 6 | 172 4 | 280 | 97 2 | 148 0 |
| 170 | 84 5 | 168 3 | 300 | 99 8 | 147 0 |
| 180 | 86 2 | 164 6 | | | |

## Acknowledgment

We are grateful to the teachers of the University Department of Physics, Vinoba Bhave University, Hazaribag, for the support and the encouragement provided for this work We are also grateful to the Department of Computer Applications of the St Columba's College, Hazaribag for the computation work. PS is further grateful to her husband Sri Ajay Kumar and the entire family for the moral and financial support provided.

### References

[1] H R Otto, H Rudigier, P Delsing and Z Fisk *Phys Rev Lett* **55** 1595 (1985)

[2] Z Fisk, D W Hess, C J Pethick, D Pines, J L Smith, J D Thompson and J O Willis *Science* **239** 33 (1988)

[3] P A Lee, T M Rice, J W Serene, L J Sham and J W Wilkins *Comments Condens Matter Phys* **12** 99 (1986)

[4] T M Rice *Phys Scr* **T19** 246 (1987)

[5] A M Awasthi, L. Degiorgi, G Gruner, Y Dalichaouch and M B Maple *Phys Rev* **B48** 10692 (1993)

[6] A J Millis and P A Lee *Phys Rev* **B35** 3394 (1987)

[7] A J Millis, M Lavagna and P A Lee *Phys Rev* **B36** 864 (1987)

[8] N W Ashcroft and N D Mermin *Solid State Physics* p 323 (India Harcourt Asia PTE Ltd ) (2001)

[9] R Freytag and J Keller *Z Phys* **B80** 241 (1990)

*Indian J. Phys.* **82 (12)** 1671-1679 (2008)

IJP

# Determination of the effective magnetic anisotropy constant of ferrite nanoparticles dispersed in organic matrix

Osaci Mihaela

Electrical Engineering and Industrial IT[1] Department, Faculty of Engineering Hunedoara, "Politehnica Timisoara" University, 5 Revolutiei Street, Zip code 331128, Romania

E-mail osaci mihaela@fih upt ro

*Received 22 April 2008, accepted 25 August 2008*

**Abstract** : With increasing interest in realising new magnetic materials, the magnetic behaviour of the nanoparticle disperse systems became an important problem both from the experimental point of view and from the theoretical one The researches performed in the last period show that, by controlling the size distribution, the effective anisotropy constant and the nanoparticle concentration, the nanoparticle disperse systems can be used for realising magnetic materials with special properties This paper presents a modality to determine the effective anisotropy constant of the mixed ferrite nanoparticle of NiZn, dispersed in the solid organic dielectric matrix – Nestrapol 450 In this respect, there are realised samples with low nanoparticle concentration, which are studied in dynamic magnetic fields through the *Q*-metric method, using a coaxial transmission line in short-circuit So, it can determine the dependence of the complex magnetic permeability components, the tangent of the magnetic loss angles and material quality factor, on the frequency, and then we can calculate the medium Néel relaxation time and the effective anisotropy constant of the nanoparticles

**Keywords :** Fine-particle systems, magnetic properties, nanoparticles, composite materials

**PACS Nos. :** 78 66 Vs, 74 25 Gz, 61 46 Df, 72 80 Tm

## 1. Introduction

For a given substance, the effective magnetic anisotropy constant depends on the method of nanoparticle generation. So, for the magnetite nanoparticles, Raiker and Shliomis [1] indicate values of this constant in the range $10^3$–$10^4$ J/m$^3$. In the same time, Kneller presents [2] values determined by many authors, refer to the effective magnetic anisotropy constant of massive samples, at room temperature. They set in the range $(7.3–14)\cdot10^3$ J/m$^3$. For the mixed ferrite nanoparticles of ferro-fluids types $Mn_{0.4}Zn_{0.6}Fe_2O_4$ and $Mn_{0.4}Zn_{0.6}Fe_2O_4$, the effective magnetic anisotropy constants have been determined [3] (values found : $1.9\cdot10^3$ J/m$^3$ and $1.3\ 10^3$ J/m$^3$). In case of mixed

ferrites, Dillon [4] indicates the value $7.2 \cdot 10^3$ J/m$^3$ for the anisotropy constant of a sintered ferrite sample of NiZn.

In the magnetisation process of a nanoparticle system dispersed into a solid matrix, the magnetic moment rotation dependents on the nanoparticle, this one remaining fixed. Owing to this mechanism, there appears a Néel relaxation moment [5] associated with the magnetic moment rotation, inside the nanoparticle, the corresponding relaxation time being correlated with the material properties of the particles. In case of a low nanoparticle concentration, so that we can neglect the dipole magnetic interactions among the nanoparticles, the expression of the Néel relaxation time has been established by Brown, in the form [5] :

$$\tau_N = \tau_{0N} \exp\left(\frac{KV}{k_B T}\right), \tag{1}$$

where $V$ is the volume of the particle magnetic core. In the relation (1), based on the study presented in the paper [2] :

$$\tau_{0N} = \sqrt{\frac{\pi}{4\sigma^3}} \cdot \tau_{Bi}, \tag{2}$$

where $\sigma = \frac{KV}{k_B T}$, $K$ = effective magnetic anisotropy constant of the nanoparticles, $V$ = average volume of the nanoparticle, $k_B$ = Boltzmann constant, $T$ = absolute temperature, and $\tau_{Bi}$ = relaxation time "inherent Brown", introduced due to the analogy between the rotation motion of the magnetic moments, inside the particle, and the Brown rotation of the particle :

$$\tau_{Bi} = \frac{3\eta_m V}{k_B T}, \tag{3}$$

where $\eta_m$ is "the internal magnetic viscosity" which depends on the nature of the material. Replacing (3) in (2) and taking into account the expression of the non-dimensional ratio $\sigma$, it results :

$$\tau_{0N} = \frac{3\eta_m}{2K}\sqrt{\frac{\pi k_B T}{KV}}. \tag{4}$$

The motion of the magnetic moments in the magnetic field $\boldsymbol{H}$, *versus* the crystal axes of the particles, is described by the equation Landau-Lifschitz [1] :

$$\frac{d\boldsymbol{m}}{dt} = -\gamma(\boldsymbol{m} \times \mu_0 \boldsymbol{H}) - \frac{\alpha\gamma}{m}\left[\boldsymbol{m} \times (\boldsymbol{m} \times \mu_0 \boldsymbol{H})\right], \tag{5}$$

where $\alpha$ is a non-dimensional damping constant and $\gamma$ is a gyromagnetic factor. In a constant field, the first term (from right) of the relation (5) represents the free

precessional motion of the magnetic moments around the ***H*** direction with Larmor frequency $\omega_L = \gamma\mu_0 H$ The second term, which represents a vector directed from the magnetic moment direction to the applied field direction, determines the reduction of the precession angle The time when the magnetic moments direction overlaps the field direction is exactly the Neel relaxation time $\tau_N$ The factor $b_r = \frac{\alpha\gamma}{\mu_0 m}$ in the relation (5) represents the rotational mobility of the magnetic moments Therefore, for the rotational diffusion coefficient of the vector ***m***, according to Einstein's formula [2], we have $D_r = b_r k_B T = \frac{\alpha\gamma k_B T}{\mu_0 m}$ Taking into account the definition of the diffusion time $\tau_{Br} = (2D_r)^{-1}$ and the relation for the magnetic field of the monodomain particle ($m = VM_s$, where $M_s$ is the saturation magnetisation of the solid material which the particle comes from), we obtain .

$$\tau_{Br} = \frac{\mu_0 M_s V}{2\alpha\gamma k_B T}. \tag{6}$$

From (3) and (6), we get the explicit expression for the magnetic viscosity

$$\eta_m = \frac{\mu_0 M_s}{6\alpha\gamma} \tag{7}$$

By introducing (7) in (4), for $\tau_{0N}$ we obtain the expression

$$\tau_{0N} = \frac{\sqrt{\pi}}{2}\ \tau_0 \sigma^{1/2} \tag{8}$$

with

$$\tau_0 = \frac{\mu_0 M_s}{2\alpha\gamma K} = (\alpha\omega_L)^{-1} \tag{9}$$

which represents the relaxation time of the precessional motion in the anisotropy field $H_a$. If, at the moment $t = 0$, the vector ***m*** deviates from the low magnetisation direction with an angle $\theta_0$, then, under the action of the anisotropy field, the angle between ***m*** and $\boldsymbol{H_a}$ varies in time, according to the relation .

$$\theta(t) = \theta_0 \exp \tag{10}$$

If we introduce (8) in (1), we obtain the Néel relaxation time [5]

$$\tau_N = \tau_{0N}\ \exp\sigma = \frac{\sqrt{\pi}}{2}\ \tau_0\ \sigma^{-\frac{1}{2}} \exp\sigma\,, \tag{11}$$

where $\tau_0$ is given by the relation (9) and $\sigma = \frac{KV}{k_B T}$.

The relaxation processes involve dissipative processes that are described by the dependence of the imaginary component $\chi''$ of the complex magnetic susceptibility on the field frequency. According to Debye [6], the Néel relaxation time is correlated with the angle frequency $\omega_{max}$, where $\chi''$ is maximum according to the relation :

$$\omega_{max}\tau_N = 1. \quad (12)$$

As example, we will realise a sample with low concentration of mix ferrite NiZn. Through a *Q*-metric method, using a line with short-circuit transmission as sample, we will determine the dependence of the imaginary component $\chi''$, complex magnetic susceptibility or the imaginary component of the complex magnetic permeability $\mu''$ on the applied field frequency. From the dependence graph $\mu'' = f(f)$, we will determine the frequency that corresponds to the peak of the curve. We will introduce the value of this frequency in the Debye relation (12) to determine the average Néel time for the magnetic relaxation and then, from the relation (11), through graphical plotting, we will determine the effective average magnetic anisotropy constant of the nanoparticles.

## 2. Sample preparation

The sample is made of nanometric dielectric ferrite powders, having organic nature. The nanometric powder is mix ferrite NiZn, $Ni_{0,2}Zn_{0,8}Fe_2O_4$, obtained through atomisation, with the average magnetic diameter of 13 nm, having spontaneous magnetisation $M_s$ = $2.85 \cdot 10^5$ A/m. The used organic matrix is Nestrapol 450, an unsaturated polyester resin in liquid state. During mixing and homogenising the powder-Nestrapol mixture, we added a plasticiser – cobalt naphthenate and a hardener – butanox (peroxide of methyl-ketone), and then the mixture was poured in moulds. The mixture solidified in the moulds in few hours, at the room temperature, depending on hardener quantity. We obtained a toroid sample, with the length smaller than the length of the coaxial transmission line used in the measuring installation. The apparent volumetric fraction (the volume occupied by the unpressed powder spread in the sample volume) is 0.7335 and the real one is 0.3836.

## 3. Method for measuring the complex magnetic permeability in a radiofrequency field

### *Experimental results*

To determinate the components of the complex magnetic permeability, we used a *Q*-metric method [7] based on the determination of the complex impedance of the sample, $z_s = R_s + jX_s$ with the help of the short-circuit transmission coaxial line technique. In case the transmission line is not full of material, the method presented

in [3] and [8] may be used, applied for fluids. The equivalent circuit of the short-circuit transmission coaxial line, discharged on the charge impedance $z_s$ is presented in Figure 1, and the line model is presented in Figure 2.

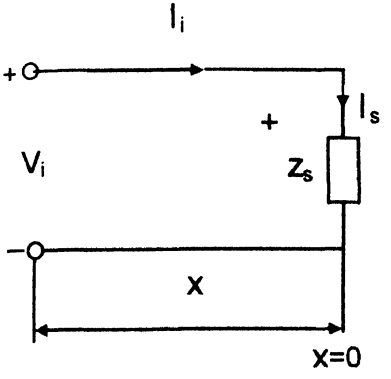


**Figure 1.** The equivalent circuit of the transmission line discharged on the charge impedance $z_S$.

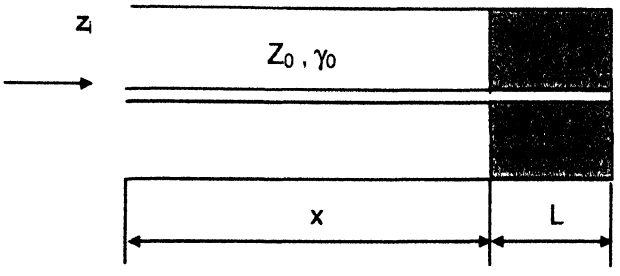


**Figure 2.** The model of the transmission coaxial line in short-circuit, discharged on a toroid sample.

The feed impedance of the transmission line at the distance $x$ from the charge (Figure 1) is given by :

$$z_i = \frac{V_i}{I_i} = \frac{V_s \cosh(\gamma_0 x) + z_0 I_s \sinh(\gamma_0 x)}{I_s \cosh(\gamma_0 x) + \frac{V_s}{z_0} \sinh(\gamma_0 x)} . \tag{13}$$

That can be written as :

$$z_i = z_0 \frac{z_s + z_0 th(\gamma_0 x)}{z_0 + z_s th(\gamma_0 x)} , \tag{14}$$

where $z_0$ is the characteristic impedance of the empty line (with air) with

$$z_0 = \frac{z_{m0}}{2\pi} \ln \frac{D}{d} = \sqrt{\frac{\mu_0}{\varepsilon_0}} \cdot \frac{1}{2\pi} \ln \frac{D}{d} , \tag{15}$$

where $D$ and $d$ are the outer and, the respective, inner diameter of the transmission line, and $\gamma_0$ is the propagation constant that can be written :

$$\gamma_0 = \alpha + j\beta \tag{16}$$

with $\alpha \rightarrow$ the attenuation coefficient, $\beta = 2\pi/\lambda \rightarrow$ phase factor and $\lambda \rightarrow$ wavelength in line. In case the losses in line are very low $\alpha \cong 0$ and $\gamma_0 = j\beta$, the eq. (14) becomes :

$$z_i = z_0 \frac{z_s + j z_0 tg(\beta x)}{z_0 + j z_R tg(\beta x)} . \tag{17}$$

In the methods presented in the papers [3] and [8], the relation used is type (17). Thenceforth, we will take into account also the attenuation coefficient from the propagation constant. In case of coaxial air line in short-circuit, with the length $l$, $z_s = 0$ and $V_s = 0$. And, from the relation (14), the feed impedance becomes :

$$z_{l0} = z_0 th(\gamma_0 l). \tag{18}$$

From the relation (18), using the expression of the hyperbolic tangent,

$$th(\gamma_0 l) = \frac{e^{\gamma_0 l} - e^{-\gamma_0 l}}{e^{\gamma_0 l} + e^{-\gamma_0 l}}, \tag{19}$$

we obtain the propagation constant for the air line :

$$\gamma_0 = \frac{1}{2l} \ln \frac{z_{l0} + z_0}{z_0 - z_{l0}}. \tag{20}$$

Let's consider the case of a discharge coaxial transmission line, on a sample with the length $L$ (Figure 2), where $z_0$ and $\gamma_0$ represent the characteristic impedance and the propagation constant for the air line. From the relation (14) we obtain :

$$z_s = z_0 \frac{z_l - z_0 th(\gamma_0 x)}{z_0 - z_l th(\gamma_0 x)}, \tag{21}$$

$$z_l = R_l + jX_l. \tag{22}$$

The values measured through the $Q$-metric method, $Q_1$, $C_1$, $Q_2$, $C_2$, for the coaxial line partially filled with magnetic material (Figure 2), are used in the relations [3], [8] :

$$R_l = \frac{1}{2\pi f}\left(\frac{1}{C_l Q_l} - \frac{1}{C_0 Q_0}\right), \tag{23}$$

$$X_l = \frac{1}{2\pi f}\left(\frac{C_0 - C_l}{C_0 C_l}\right). \tag{24}$$

For $i = 1$, without the sample, we obtain $Ri_0$ and $Xi_0$, and for $i = 2$, with the sample presence, we obtain the components $R_{ip}$ and $X_{ip}$ of the charge seen through the line with the length $l$. By gradually introducing the value pairs ($R_{ip}$, $X_{ip}$) and ($R_{i0}$, $X_{i0}$) in the relation (9) that takes into account the losses, inspite of the ideal relation (17), we obtain the impedance components of the line segment (with magnetic material),

$$z_{x_p} = R_{x_p} + jX_{x_p}, \text{ şi } z_{x_0} = R_{x_0} + jX_{x_0}, \tag{25}$$

Then, the real component of the magnetic permeability is $\mu' = \frac{X_{x_p}}{X_{x_0}}$, the tangent of the magnetic losses angle is $tg\delta_m = \frac{R_{x_p} - R_{x_0}}{X_{x_p}}$, the imaginary component of the magnetic

permeability is : $\mu'' = (\mu' + 1)tg\delta_m$ and the factor of material quality is $Q = \frac{1}{tg\delta_m}$. Experimental results for our sample are presented in Figure 3.

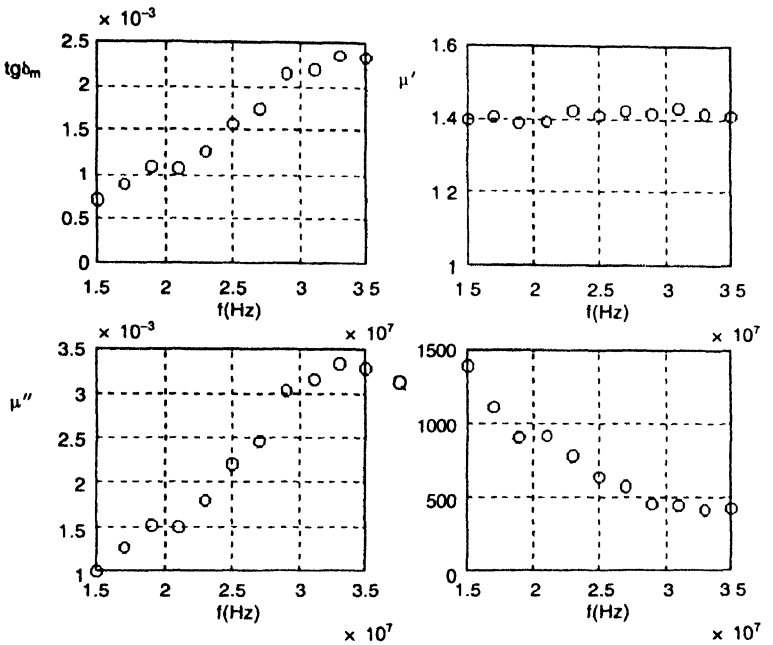


**Figure 3.** The tangent of the losses angle, the complex relative components of the magnetic permeability and the quality factor of the material are plotted against the frequency – for our sample.

Theoretically (Debye theory), it was shown that at the frequency when $\chi''$ is maximum, the condition : $\chi_m'' = \chi_m'$ is effective, where $\chi_m'$ represents the value of $\chi'$ at the same frequency. But, after measurements, it was seen that $\mu_m'' < \mu_m'$, *i.e.* $\chi_m'' < \chi_m'$. This kind of deviation can be explained by the fact that only some particles of the magneto-dielectric material have a super paramagnetic behaviour. In Figure 3, it can be seen that the maximum imaginary component of the complex magnetic permeability is obtained at an average frequency of 34 MHz that corresponds, according to Debye relation, at the Néel relaxation time $\tau_N$ = 4.68 ns.

In order to determine the anisotropy effective constant of the sample nanoparticle, the Néel relaxation time (11) should be written [having in view also the relation (9)], as follows :

$$\frac{a \cdot \exp(b \cdot K)}{\tau_N \cdot K \cdot \sqrt{K}} = 1, \tag{26}$$

where $a = \frac{\mu_0 M_s \sqrt{\pi k_B T}}{4\alpha\gamma\sqrt{V}}$ and $b = \frac{V}{k_B T}$ are constants that can be calculated taking into

account the value of the giromagnetic factor $\gamma = 2.41 \cdot 10^5 s^{-1} A^{-1} m$ and the damping constant $\alpha = 0.02$ (for most ferromagnetic materials, $\alpha$ is around $10^{-2}$). The relation (26) is a transcendental equation in the unknown $K$, whose solution can be graphically determined. Let $f_1$ be the numerator of the relation (26) and $f_2$ the denominator of the relation (26). At the room temperature, the graphical representation of the functions $f_1$ and $f_2$ is presented in Figure 4. The solution (the value of $K$) is the value where the two curves intercross (*i.e.* $K$ = 6300 J/m$^3$).

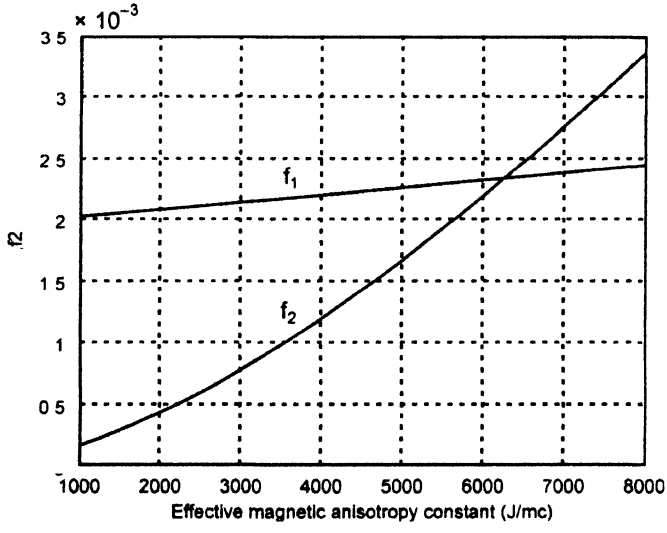


**Figure 4.** The graphical determination of the effective magnetic anisotropy constant of the mixed NiZn ferrite nanoparticles dispersed in solid organic dielectric matrix.

If we consider the particles to be spherical, identical and arranged into a cube tangent to nanoparticles, the maximum volumetric real fraction of nanoparticles, in case the powder is not pressed, is $f_{max}$ = 0.523. According to Garcia relation [9], the maximum volumetric real fraction of nanoparticles, in case the powder is not pressed, is $f_m \quad 0.32 \cdot \frac{8K\pi}{\mu_0 M_s^2} = 0.523$, where $\mu_0$ is the vacuum magnetic permeability. From this relation, we obtain a limit for $K$ = 6637 J/m$^3$. It can be seen that there is a good correspondence with the value determined through the graphical method. The difference, between this value and the graphically obtained value, can be explained by the fact that the dispersed nanoparticles in Nestrapol 450 are not perfectly spherical.

## 4. Conclusions

The paper presents an experimental study of a composite material, in dynamic radiofrequency field, based on mixed NiZn ferrite nanoparticles and, in the same time, a method to determine the effective magnetic anisotropy constant of the nanoparticles dispersed in an organic dielectric solid matrix. The method takes into account the fact

that $\tau_{0N}$ (from the Néel relaxation time relation) depends on $K$ [relation (9)] and it is not considered a constant with the value of $10^{-9}$ seconds, inspite of the claims in literature.

The scientific and technological importance of the dispersed magnetic systems of nanometric particles is justified by the possibility of realising advanced magnetic materials [10–16], from natural nanostructures to artificial nanostructures : ferro-fluids, medium of high density magnetic recording, magnetic sensors, hard and soft magneto-dielectric electro-technical materials, at usual and high frequencies ..

In all these cases, the special magnetic properties of the materials can be obtained through an adequate check of the effective magnetic anisotropy constant and the distribution of nanoparticle dimensions and concentration [17]

**References**

[1] Y L Raikher and M I Shliomis *Adv Chem Phys* **87** ch 8 (1994)

[2] E Kneller *Ferromagnetisms* (Berlin Springer Verlag) (1962)

[3] I Mălăescu *Ferrofluids in Radiofrequency Field* (Timişoara Publishing House MIRTON) (1998)

[4] J F Dillon and M E Earl *J Appl Phys* **30** (1958)

[5] M F Hansen and S Mørup *JMMM* **184** 262 (1998)

[6] P Debye *Polar Molecules* (New York The Chemical Catalog Company) (1929)

[7] I Hrianca and I Mălăescu *J Magn Magn Mater* **150** 131 (1995)

[8] P C Fannin, T Relihanşi and S W Charles *J Appl Phys* **23** 2003 (1995)

[9] J Garcia-Otero, M Porto, J Rivas and A Bunde *Physical Review Letters* **84** nr 1, 167 (2000)

[10] A L Babichevchev and G G Krylov *Nonlinear Phenomena in Complex System* **7** 298 (2004)

[11] F J Himpsel, J E Ortega, G J Mankey and R F Willis *Advansed in Physics* **47** 511 (1998)

[12] R Skomski *J Phys Condens Matter* **15** R841 (2003)

[13] J Fidler and T Schrefl *J Appl Phys* **33** R135 (2000)

[14] Z Zhang and K Friedrich *Composites Science and Technology* **63** 2029 (2003)

[15] A B Bortz, M H Kalos and J L Lebowitz *J Computational Physics* **17** (1975)

[16] S V Nemkov and T R Ruffini *International Symposium in Product Development in Engineering Education, Halmstad University, Sweden* (1996)

[17] Osaci Mihaela, Abrudean Cristian and Berdie Adela *Acta Physica Polonica* A **112** nr 6, 1203 (2007)

*Indian J. Phys.* **82 (12)** 1681-1687 (2008)

IJP

# Asymmetric group velocity dispersion and pulse distortion in a uniform fiber Bragg grating

Sanjeev Kumar Raghuwanshi* and Srinivas Talabattula

Applied Photonics Laboratory, Department of Electrical Communication Engineering, Indian Institute of Science, Bangalore-560 012, India

E-mail sanjeevkr@ece.iisc.ernet.in

*Received 2 March 2008, accepted 4 July 2008*

**Abstract** : In a uniform fiber Bragg grating, if the input signal is a Gaussian pulse the dispersion is zero near center wavelength and becomes appreciable only near the band edges and side lobes of the reflection spectrum However for chirped Gaussian pulses, group velocity dispersion and the reflected light must become asymmetric Here the chirped Gaussian pulses can be treated as a symmetric but nonuniform input signal The present paper describes that for the case of symmetric Gaussian pulse, the group velocity dispersion and pulse distortion remain symmetric however strong the grating may be On the other hand both tend to be more asymmetric for the case of strong grating while the input signal is symmetric with nonuniform shape

**Keywords** : Coupled mode theory of fiber Bragg gratings, group velocity dispersion effect, chirped Gaussian pulses

**PACS Nos.** : 42.79.Dj, 42 79 -e

## 1. Introduction

Recently, there has been growing interest in the dispersive properties of fiber Bragg gratings for applications such as dispersion compensation, pulse shaping and fiber and semiconductor laser components [1]. Although many of these rely on the ability to tailor the dispersion in the nonuniform gratings, here we introduce the basis for determining delay and dispersion from the known (complex) reflectivity of a uniform Bragg grating. The amplitude and power reflection coefficients in a uniform fiber Bragg grating for the case of non-phase-matched contradirectional modes coupling are given by [2–14] :

$$\rho|_{z=0} = \frac{-\kappa \sinh(\Omega L)}{\frac{\Gamma_1}{2}\sinh(\Omega L) + j\Omega \cosh(\Omega L)}, \tag{1}$$

*Corresponding Author

$$|\rho|^2 = \frac{\left[\Omega^2 + \left(\frac{\Gamma_1}{2}\right)^2 \sinh^2(\Omega L)\right]}{\Omega^2 \cosh^2(\Omega L) + \left(\frac{\Gamma_1}{2}\right)^2 \sinh^2(\Omega L)}. \tag{2}$$

Here the parameters $\Gamma_1$, $k$ and $\Omega$ represent the mismatch between the momentum of the mode with the refractive index perturbation, mode coupling coefficient and the phase detuning parameter, respectively. Turan Erdogan [2] presents a derivation of the above equations. The group delay and dispersion of the reflected light can be determined from the phase of the amplitude reflection coefficient [2]. If we denote $\theta_\rho \equiv phase(\rho)$ then, the delay time $\tau_\rho$ for light reflected off a grating is

$$\tau_\rho = \frac{\theta_\rho}{d\omega} = -\frac{\lambda^2}{2\pi c}\frac{d\theta_\rho}{d\lambda}. \tag{3}$$

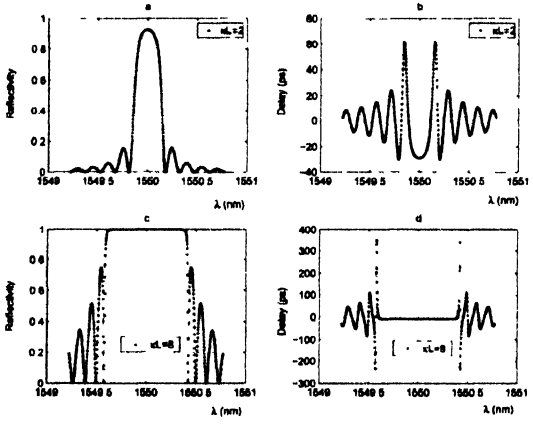


**Figure 1.** Calculated reflection spectra and corresponding group delay for an uniform Bragg grating with (a), (b) $\kappa L = 2$ and (c), (d) $\kappa L = 8$.

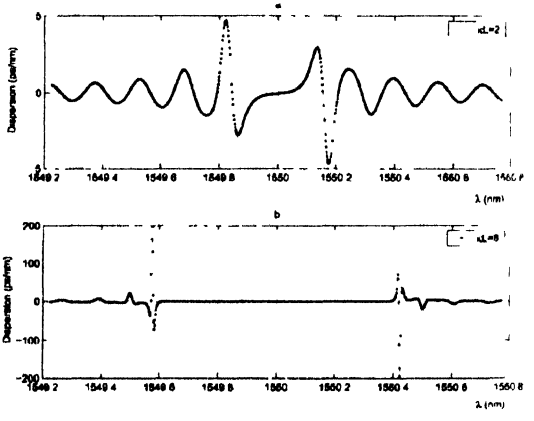


**Figure 2.** Calculated group velocity dispersion for the same case as Figure 1 with (a) $\kappa L = 2$ and (b) $\kappa L = 8$.

Figure 1 shows the delay $\tau_\rho$ calculated for the two examples of the grating. We see that for unchirped uniform grating both the reflectivity and delay are symmetric about the center wavelength. Since the dispersion $d_\rho$ (in ps/km) is the rate of change of delay with wavelength, we find

$$d_\rho = \frac{d\tau_\rho}{d\lambda}$$

$$= \frac{2\tau_\rho}{\lambda} - \frac{\lambda^2}{2\pi c}\frac{d^2\theta}{d\lambda^2}$$

$$= -2\pi c\lambda^2 \frac{d^2\theta_p}{d\omega^2} \tag{4}$$

In a uniform grating, the dispersion is zero near center wavelength as shown in Figure 2 and becomes appreciable only near the band edges and side lobes of the reflection spectrum, where it tends to vary rapidly with wavelength.

## 2. Asymmetric pulse distortion

Gaussian pulses can be considered as a symmetric signal, on the other hand chirped Gaussian pulses can be presumed to be nonuniform but symmetric signal. Figure 3 demonstrates various kinds of Gaussian pulses with different values of chirp parameter [3]. Now if we feed these Gaussian pulses to a uniform Bragg grating, we can visualize the pulse distortion as well as reflected mode field due to these chirp factors. We consider only the positive chirped Gaussian pulses into analysis because the negative chirp factor will only reverse the whole effect. First we present the results of chirp free pulses. Figure 4 shows the fundamental reflected mode field and corresponding peak power reflection spectrum.

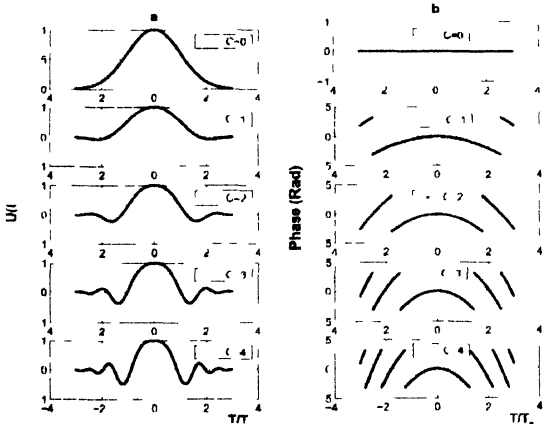


**Figure 3.** Gaussian pulses (left side) and corresponding phase spectrum (right side) for various values of chirp factor.

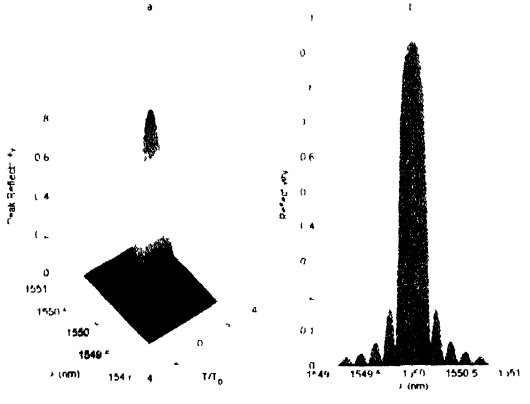

**Figure 4.** Fundamental reflected mode field and corresponding peak power reflection spectrum while $C = 0$ and $\kappa L = 2$

Figures 5 and 6, show the reflected light for the two cases, one for weak grating ($\kappa L = 2$) and another for strong grating ($\kappa L = 6$), while chirping factor is kept at $C = 0$ and $C = 2$, respectively. One can see from Figures 5 and 6 that for chirp free pulses the reflected power is symmetric in both the cases, while for $C = 2$, they are considerably asymmetric. Reflected pulse would be more asymmetric for strong grating.

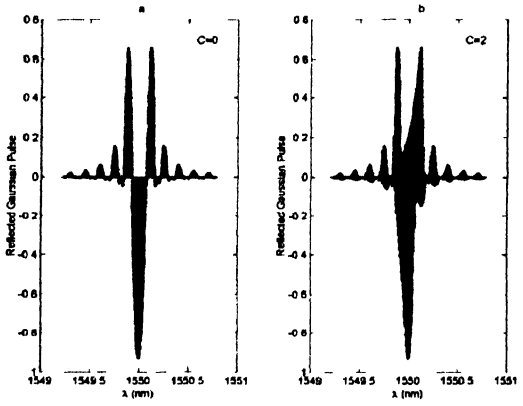


**Figure 5.** Reflected light at $z = 0$, while (a) $C = 0$, (b) $C = 0$ and $\kappa L = 2$

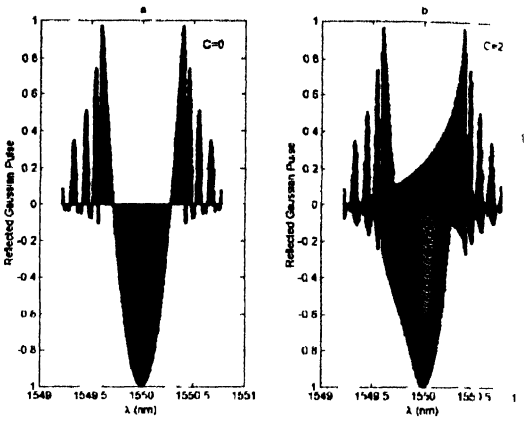


**Figure 6.** Reflected light at $z = 0$, while (a) $C = 0$ (b) $C = 2$ and $\kappa L = 8$

## 3. Asymmetric group velocity dispersion

Dispersion plots and corresponding contour maps for various values of chirp factors are shown in Figures 7, 8 and 9, respectively for $\kappa L = 2$. For the case of chirp free pulse

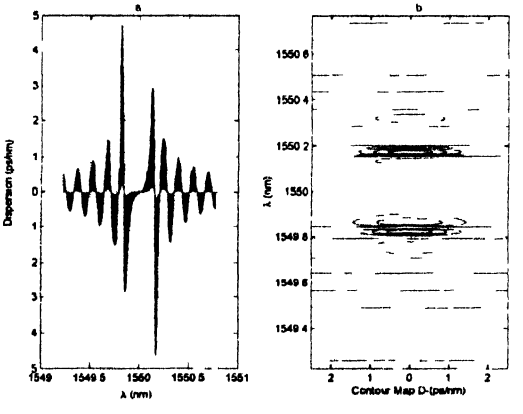


**Figure 7.** Dispersion and corresponding contour map for $C = 0$ and ($\kappa L = 2$)

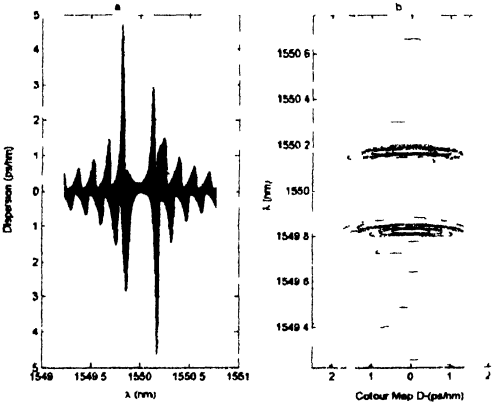


**Figure 8.** Dispersion and corresponding contour map for $C = 2$ ($\kappa L = 2$)

the dispersion is zero at center wavelength where the peak reflection occurs; on the other hand, for considerably chirped pulses the dispersion curve no longer remains symmetric but picks up a considerable curvature. For highly chirped Gaussian pulses ($C = 4$), the dispersion curve picks up larger curvature at all the wavelength of interest This feature can be considered as an asymmetric response of uniform fiber Bragg grating even for weak grating case. Figures 10 and 14 show the fundamental reflected mode field and corresponding peak power reflection spectrum for the case of moderately strong ($\kappa L = 4$) and strong grating ($\kappa L = 6$). The reflection bandwidth of the spectrums are 0.4 nm (Figure 10) and 0.6 nm (Figure 14), respectively. Dispersion and contonr maps for different values of $C$ and $\kappa L$ are displayed in Figures 11–13. Comparison of

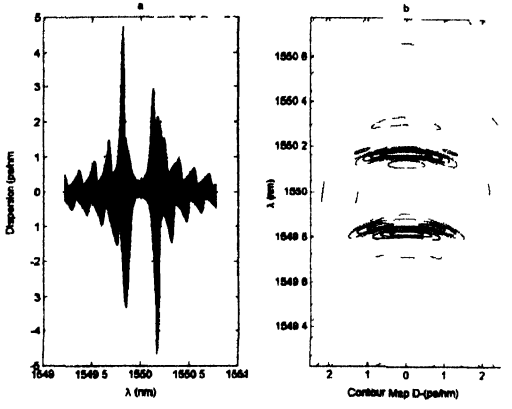


**Figure 9.** Dispersion and corresponding contour map for $C = 4$ ($\kappa L = 2$)

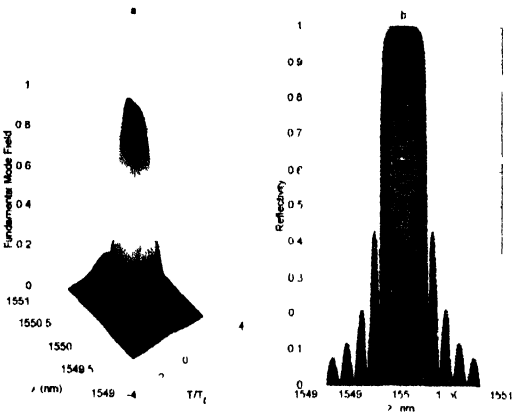


**Figure 10.** Fundamental reflected mode field and corresponding peak power reflection spectrum while $C = 0$ and $\kappa L = 4$

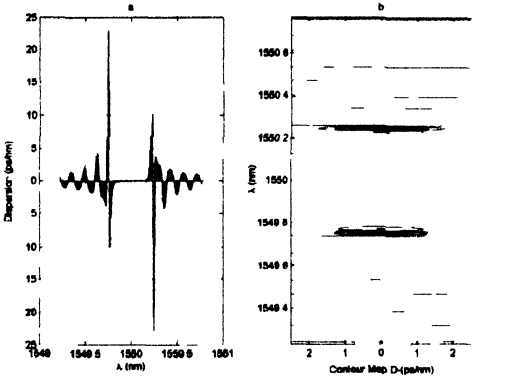


**Figure 11.** Dispersion and corresponding contour map for $C = 0$ ($\kappa L = 4$)

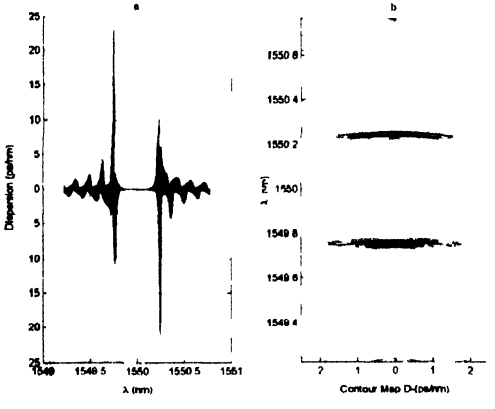


**Figure 12.** Dispersion and corresponding contour map for $C = 2$ ($\kappa L = 4$)

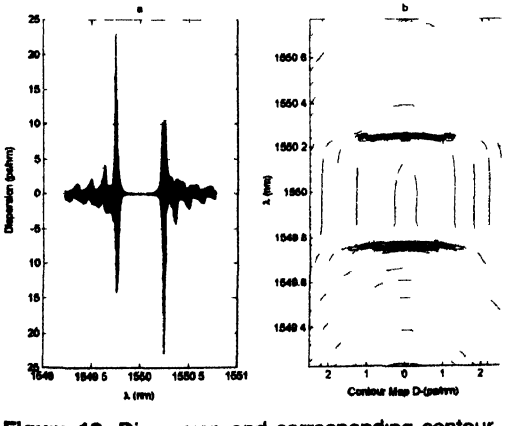


**Figure 13.** Dispersion and corresponding contour map for $C = 4$ ($\kappa L = 4$)

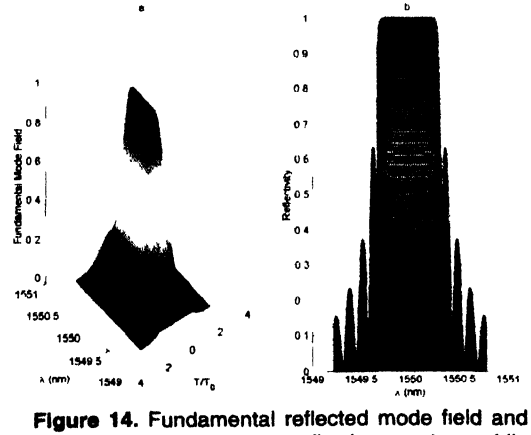


**Figure 14.** Fundamental reflected mode field and corresponding peak power reflection spectrum while $C = 0$ and $\kappa L = 6$

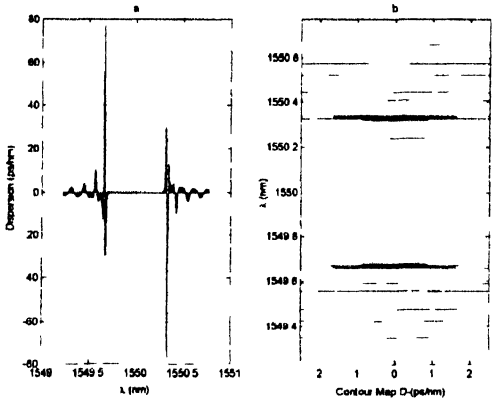


**Figure 15.** Dispersion and corresponding contour map for $C = 0$ ($\kappa L = 6$)

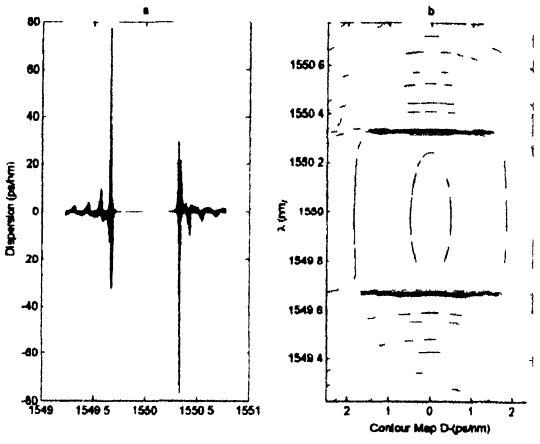


**Figure 16.** Dispersion and corresponding contour map for $C = 2$ ($\kappa L = 6$)

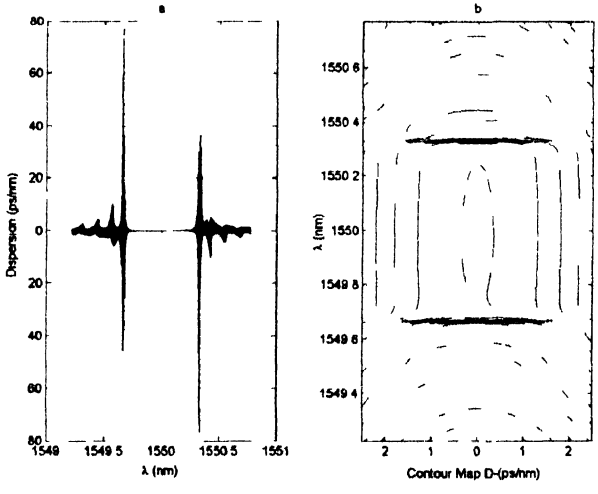


**Figure 17.** Dispersion and corresponding contour map for $C = 4$ ($\kappa L = 6$)

Figures 7, 11 and 15 suggests that for the case of symmetric Gaussian pulse the zero dispersion bandwidth is more pronounced for the case of strong grating (B.W. $\approx$ 0.6 nm) [15] while for chirp free pulses dispersion accumulates more for some singular points in the case of a strong grating (±80 ps/nm). The dispersion graph becomes significantly asymmetric for strong grating for considerably chirped Gaussian pulses. It is quite symmetric for weak grating (±5 ps/nm) case even for the same simulation parameters.

## 4. Conclusion

We have found that for the case of strong grating the dispersion is large at some particular point of bands which may be due to rapid phase variations. Infact, the weak

grating shows lesser dispersion but the dispersion is more spread out over the band as compared to strong grating The dispersion graph tends to be more asymmetric for the strongly chirped pulses. Simulation also shows that the dispersion is high due to strong grating at some singular point of wavelength There is no effect of chirp factor on absolute value of dispersion as such The only advantage of using strong grating for chirp free pulse is that we can achieve a large band of zero dispersion at some center wavelength where the peak reflection occurs

**References**

[1] F Ouellette *Optics Letters* **16** 847 (1987)

[2] T Erdogan *IEEE J Lightwave Technol* **15** 1277 (1997)

[3] G P Agarwal *Nonlinear Fiber Optics* (New York Academic) (2001)

[4] A Othonos and K Kalli *Fiber Bragg Gratings Fundamentals and Applications in Telecommunications and Sensing* (London Artech House) (1999)

[5] K O Hill *IEEE J Lightwave Technol* **15** 1263 (1997)

[6] L R Chen, S D Benjamin, P W E Smith and J E Sipe *IEEE J Lightwave Technol* **15** 1503 (1997)

[7] C R Giles *IEEE J Lightwave Technol* **15** 1391 (1997)

[8] J E Sipe, B J Eggleton and T A Strasser *Opt Commun* **15** 269 (1998)

[9] A Carballar, M A Muriel and J Azana *IEEE Photon Technol Lett* **11** 694 (1999)

[10] S K Liaw, K P Ho, Y K Chen and C C Lee *Optical and Quantum Electronics* **31** 77 (1999)

[11] Stefano Longhi *Phys Rev* **E64** 037601 (2001)

[12] S Longhi, M Marano, P Laporta, O Svelto and M Belmonte *J Opt Soc Am* **B19** 2742 (2002)

[13] Jaejoong and Byoungho Lee *IEEE Photon Technol Lett* **17** 408 (2005)

[14] Stefano Longhi *Phys Rev* **E72** 056614 (2005)

[15] S K Raghuwanshi and S Talabattula *J Instrum Soc India* **37** 297 (2007)

plasmas. The study of these effects has been paid a great deal of interest in recent years. Dust charge variations play an interesting role in the non-linear propagation characteristics of dust acoustic wave. In case of non-adiabatic dust charge variation, it produces an anomalous dissipation that causes shock wave in dusty plasmas [4,5]; also for weak dissipation, the non-linear waves become damped due to the dust charge variations [6–8].

DAWs have been studied in dusty plasmas with non-thermal ions and constant dust charge [9]. Also, these waves in hot dust plasmas have been investigated in [10]. Wang *et al* have studied effect of negative ions on the formation of solitary waves in dusty plasmas by using the Sagdeev potential [11,12]. Cylindrical KP equation in warm dusty plasmas with two ions has been studied too [13]. Solitary waves of the KdV equation have been investigated in dusty plasmas with variable dust charge in [14,15]. Gill *et al* have also analyzed solitons of KP equation for these plasmas with two temperature ions [16]. This paper deals with the 2D non-linear structures of dust acoustic waves incorporating dust charge variations and non-thermal ions. The problem is interesting from astrophysical point of view, as the observations of PHOBOS and NOZOMI satellites confirm the presence of non-thermal ions on the upper ionosphere of Mars and in the vicinity of Moon. Also in truly dusty plasma the charge on dust grains is an extra dynamical variable that varies in time.

We study the non-linear waves in dusty plasmas with variable dust charge; Boltzmann distributed electrons and the non-thermal ions. In Section 2 the basic set of equations is introduced. We will derive the KP equation by using the reductive perturbation method in Section 3. In Section 4 the modified KP equation is derived at the critical density. Finally, conclusions are given in Section 5.

## 2. Basic equations

As before mentioned, we consider the propagation of dust acoustic waves in a collisionless, unmagnetized dusty plasma consisting of high negatively charged dust grains, variable dust charges, non-thermal ions and Boltzmann distributed electrons. Total charge neutrality at equilibrium requires that $Z_{0d}n_{0d} + n_{0e} = n_{0i}$, where $n_{0i}$, $n_{0e}$ and $n_{0d}$ are the equilibrium values of ions, electrons and dust number densities respectively. $Z_{0d}$ is the unperturbed number of charges on the dust particles. The following set of normalized two dimensional equations of motion describe the dynamics of dust acoustic wave in the variable dust charge plasmas :

$$\frac{\partial n_d}{\partial t} + \frac{\partial}{\partial x}(n_d u_d) + \frac{\partial}{\partial y}(n_d \nu_d) = 0, \quad \frac{\partial u_d}{\partial t} + u_d \frac{\partial u_d}{\partial x} + \nu_d \frac{\partial u_d}{\partial y} = Z_d \frac{\partial \phi}{\partial x}$$

$$\frac{\partial \nu_d}{\partial t} + u_d \frac{\partial \nu_d}{\partial x} + \nu_d \frac{\partial \nu_d}{\partial y} = Z_d \frac{\partial \phi}{\partial x}, \quad \frac{\partial^2 \phi}{\partial x^2} + \frac{\partial^2 \phi}{\partial y^2} = Z_d n_d + n_e - n_i \tag{1}$$

in which $u_d$ and $\nu_d$ are velocity components of the dust particles in $x$ and $y$-directions

and normalized by the dust acoustic speed $c_d = \sqrt{Z_{0d}T_i/m_d}$, where $T_i$ is the temperature of ions, $m_d$ is the mass of dust particles. $n_d$ and $\phi$ are the dust number density and electrostatic potential that have been normalized by $n_{0d}$ and $T_i/e$ and $e$ is the magnitude of the electron charge, respectively. $n_e$ and $n_i$ are the electron and ion number densities which are normalized by $n_{0e}$ and $n_{0i}$, respectively. The space and time variables are normalized by the Debye length $\lambda_D = \sqrt{T_i/4\pi n_{0d}Z_d e^2}$ and the inverse of dust plasma frequency $\omega_{pd}^{-1} = \sqrt{m_d/4\pi n_{0d}Z_{0d}^2 e^2}$, respectively. Normalized number densities for Boltzmann distributed electrons and non-thermal distributed ions are

$$n_e = (\mu/1-\mu)\, e^{\sigma_i\phi}, \qquad n_i = (1/1-\mu)\left[1+\beta\left(\phi+\phi^2\right)\right] e^{-\phi} \tag{2}$$

where $\mu = n_{0e}/n_{0i}$, $\sigma_i = T_i/T_e$ and $\beta = 4\alpha/(1+3\alpha)$ in which $\alpha$ arises due to the effects of non-thermal ions. The electron and ion currents for spherical dust grains with radius $r$ are [17]

$$I_e = -e\pi r^2\sqrt{8T_e/\pi m_e}\left(\frac{\mu}{1-\mu}\right) e^{\sigma_i(\phi-\psi)}$$

$$I_i = -e\pi r^2\sqrt{8T_i/\pi m_i}\left(\frac{1}{1-\mu}\right)\left(\frac{1}{1+3\alpha}\right)$$

$$\times\left\{\left[\left(1+\frac{24\alpha}{5}\right)+\frac{16\alpha}{3}\phi+4\alpha\phi^2\right]-\psi\left[\left(1+\frac{8\alpha}{5}\right)+\frac{8\alpha}{3}\phi+4\alpha\phi^2\right]\right\} e^{-\phi} \tag{3}$$

in which $\psi = ZQ_d$ denotes the dust grain surface potential relative to the plasma potential $\phi$ and $Q_d = q_d/z_d e$, where $q_d$ is the dust charge. $z_d e$ is the magnitude of the equilibrium dust charge and $Z = z_d e^2/4\pi\varepsilon_o r T_e$ is the non-dimensional dusty plasma parameter. The term $4\pi\varepsilon_0 r$ is the capacitance of the spherical dust grain with average radius $r$. By considering the only electron and ion currents due to collisions with plasma particles, the dust grain charging equation is given by

$$\partial Q_d/\partial t = \left(I_e + I_i\right)/z_d e. \tag{4}$$

If the thermal velocities of electrons and ions are larger than their streaming velocities [15,16] the charge-current balance equation reads [17]

$$\left(I_e + I_i\right)_{Q_d=-1,\,\phi=0} = 0 \tag{5}$$

and we have

$$\sqrt{\sigma_i/\mu_i}\left(\frac{1}{1+3\alpha}\right)\left[\left\{1+\frac{24\alpha}{5}+\frac{16\alpha}{3}\phi+4\alpha\phi^2\right\}-\psi\left\{1+\frac{8\alpha}{5}+\frac{8\alpha}{3}\phi+4\alpha\phi^2\right\}\right]$$

$$\times\exp(-\phi)(1-\psi)-\mu\exp\left[\sigma_i(\phi+\psi)\right]=0 \tag{6}$$

where $\mu_i = m_i/m_e \cong 1840$. $Z_d$ is defined as $Z_d = \frac{\psi}{\psi_0}$, where $\psi_0 = \psi(\phi = 0)$ is the dust suface floating potential with respect to the unperturbed plasma potential at an infinite region. By substituting $\phi$ = 0 into (5) we have

$$\sqrt{\sigma_i/\mu_i}\left(\frac{1}{1+3\alpha}\right)\left[1+\frac{24\alpha}{5}-\psi_0\left(1+\frac{8\alpha}{5}\right)\right](1-\psi_0)-\mu\exp(\sigma_i\psi_0)=0 \tag{7}$$

$Z_d$ can be expanded respect to $\phi$ as

$$Z_d = 1+\gamma_1\phi+\gamma_2\phi^2+\gamma_3\phi^3+\ldots \tag{8}$$

where $\gamma_i \equiv \frac{\psi_0'}{\psi_0}, \gamma_2 \equiv \frac{\psi_0''}{2\psi_0}$ and $\gamma_3 = \frac{1}{6}\frac{\psi_0'''}{\psi_0}$ come from expanding $\psi$ near $\psi_0$ so we can write

$$\psi_0' = \frac{\left[\frac{8\alpha}{15}-1-\psi_0\right](1-\psi_0)+\sigma_i\left[\left(1+\frac{24\alpha}{5}\right)-\psi_0\left(1+\frac{8\alpha}{5}\right)\right]}{\left[\left(1+\frac{24\alpha}{5}\right)-\psi_0\left(1+\frac{8\alpha}{5}\right)\right](1-\sigma_i(1-\psi_0))-(1-\psi_0)\left(1+\frac{8\alpha}{5}\right)} \tag{9}$$

$$\psi_0'' = \frac{\left\{\sigma_i(1+\psi_0)^2\left[1+\frac{24\alpha}{15}-\psi_0\left(1+\frac{8\alpha}{5}\right)\right]-\left[1+\frac{32\alpha}{15}+2\left(1+\frac{64\alpha}{15}\right)\psi_0'-\left(1+\frac{44\alpha}{15}\right)\psi_0\right]\right\}(1-\psi_0)}{\left[\left(1+\frac{24\alpha}{5}\right)-\psi_0\left(1+\frac{8\alpha}{5}\right)\right](1-\sigma_i(1-\psi_0))-(1-\psi_0)\left(1+\frac{8\alpha}{5}\right)}$$

and

$$\psi_0''' = \frac{A}{B},$$

where $A$ and $B$ are

$$A = \left\{2\sigma_i(1+\psi_0)^2+2\psi_0''\left[1+\sigma_i(1+\psi_0')\right]\right\}\times$$

$$\left[1+\frac{24\alpha}{5}-\psi_0\left(1+\frac{8\alpha}{5}\right)\right](1-\psi_0)\sigma_i-\psi_0''\left[\frac{8\alpha}{5}-1+\psi_0\left(1-\frac{16\alpha}{5}\right)-\psi_0'\left(1+\frac{8\alpha}{5}\right)\right]$$

$$+(1-\psi_0)\left\{-\left(3+\frac{372\alpha}{15}\right)+\left(1+\frac{88\alpha}{5}\right)\psi_0-\left(3+\frac{104\alpha}{5}\right)\psi_0'+\left(3-\frac{8\alpha}{15}\right)\psi_0''\right\}$$

$$-\psi_0'\left[\psi_0''\left(1+\frac{8\alpha}{5}\right)+2\psi_0'\left(1-\frac{16\alpha}{3}\right)+\psi_0\left(1+\frac{104\alpha}{5}\right)\right],$$

$$B=\left[\left(1+\frac{24\alpha}{5}\right)-\psi_0\left(1+\frac{8\alpha}{5}\right)\right](1-\sigma_i(1-\psi_0))-(1-\psi_0)\left(1+\frac{8\alpha}{5}\right) \tag{11}$$

## 3. Derivation of the KP equation

Let us study the behaviour of small amplitude dust-acoustic waves. The KP equation is obtained by using the reductive perturbation method. The stretched coordinates are defined by

$$\xi=\varepsilon(x-\lambda t),\ \eta=\varepsilon^2 y \text{ and } \tau=\varepsilon^2 t \tag{12}$$

where $\lambda$ is the phase velocity of waves and $\varepsilon$ is a small parameter which is characterizes the strength of the nonlinearity. Dependent variables are expanded as follows

$$n_d=1+\varepsilon^2 n_{1d}+\varepsilon^4 n_{2d}+\dots$$

$$u_d=\varepsilon^2 u_{1d}+\varepsilon^4 u_{2d}+\dots$$

$$v_d=\varepsilon^3 v_{1d}+\varepsilon^5 v_{2d}+\dots$$

$$\phi=\varepsilon^2\phi_1+\varepsilon^4\phi_2+\dots$$

$$Z_d=1+\varepsilon^2 Z_{1d}+\varepsilon^4 Z_{2d}+\varepsilon^6 Z_{3d}+\dots. \tag{13}$$

By substituting (13) into (1) and collecting the terms in the different powers of $\varepsilon$ we have

$$N_{1d}=-\frac{\phi_1}{\lambda^2},\ u_{1d}=-\frac{\phi_1}{\lambda},\ \frac{1}{\lambda^2}=\gamma_1+\frac{\mu\sigma_i+1-\beta}{1-\mu},\ \lambda\frac{\partial v_{1d}}{\partial\xi}=\frac{-\partial\phi_i}{\partial\eta}$$

$$\frac{\partial^2\phi_1}{\partial\xi^2}=Z_2+n_{2d}+Z_{1d}n_{1d}+\frac{1}{1-\mu}\left[\sigma_i\mu+(1-\beta)\right]\phi_2+\frac{1}{2(1-\mu)}\left(\mu\sigma_i^2-1\right)\phi_1^2$$

$$\frac{\partial n_{1d}}{\partial\tau}-\lambda\frac{\partial n_{2d}}{\partial\xi}+\frac{\partial}{\partial\xi}(n_{1d}u_{1d}+u_{2d})+\frac{\partial v_{1d}}{\partial\eta}=0$$

$$\frac{\partial u_{1d}}{\partial\tau}-\lambda\frac{\partial u_{2d}}{\partial\xi}+u_{1d}\frac{\partial u_{1d}}{\partial\xi}=\frac{\partial\phi_2}{\partial\xi}+Z_{1d}\frac{\partial\phi_1}{\partial\xi}. \tag{14}$$

Finally the KP equation is obtained

$$\frac{\partial}{\partial\xi}\left[\frac{\partial\phi_i}{\partial\tau}+a\phi_1\frac{\partial\phi_1}{\partial\xi}+b\frac{\partial^3\phi_1}{\partial\xi^3}\right]+c\frac{\partial^2\phi_1}{\partial\eta^2}=0. \tag{15}$$

Coefficients of non-linear and dispersion terms are

$$a = -\left[\gamma_2 + \frac{\mu\sigma_l^2 - 1}{2(1-\mu)}\right]\left[\gamma_1 + \frac{\mu\sigma_l + 1 - \beta}{1-\mu}\right]^{-3/2} + 3\gamma_1\left[\gamma_1 + \frac{\mu\sigma_l + 1 - \beta}{1-\mu}\right]^{-1/2}$$

$$-\frac{3}{2}\left[\gamma_1 + \frac{\mu\sigma_l + 1 - \beta}{1-\mu}\right]^{1/2}$$

$$b = \frac{1}{2}\left[\gamma_1 + \frac{\mu\sigma_l + 1 - \beta}{1-\mu}\right]^{-3/2}, \quad c = \frac{1}{2}\left[\gamma_1 + \frac{\mu\sigma_l + 1 - \beta}{1-\mu}\right]^{-1/2} \tag{16}$$

Figures 1 show "*a*" as function of $\mu$, $\alpha$ and $\sigma_l$. Figure 1a shows "*a*" as a function of $\mu$ and $\alpha$ with $\sigma_l$ = 0.3. In this figure we can see that with a fixed values for $\mu$, "*a*" increases when the value of non-thermal parameter ($\alpha$) is decreased. Also "*a*" gets increased with an increasing $\mu$ when $\alpha$ is fixed. In Figure 1b $\alpha$ has been thaken 0.5.

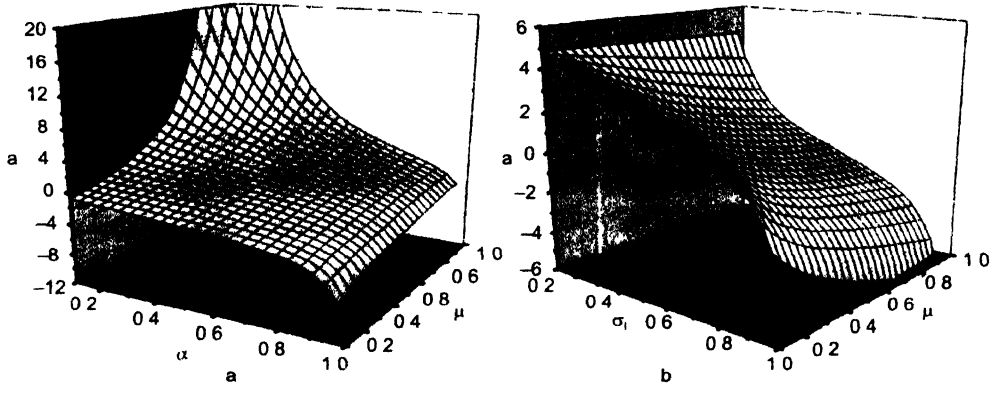


**Figure 1.** Parameter "*a*" as a function of $\alpha$, $\mu$ and $\sigma_l$ (a) $\sigma_l$ = 0 3 and (b) $\alpha$ = 0.5.

In this Figure we can see that "*a*" decreases when $\sigma_l$ is increased with fixed values for $\mu$. In all of the Figures parameters $\gamma_1$ and $\gamma_2$ have been taken equal to zero. Figures 1 show that for some values of parameters, "*a*" is positive and for some other values it is negative. This means that both compressive and rarefactive solitons are available.

Figures 2 present the parameter "*b*" respect to $\mu$, $\alpha$ and $\sigma_l$. In the *b*–$\mu$ plot $\sigma_l$ = 0.3, while in the *b*–$\sigma_l$, $\alpha$ = 0.3 and in the *b*–$\alpha$ plot $\sigma_l$ = 0.3 has been selected. The $\gamma_1$ and $\gamma_2$ are zero in all the cases. Behaviour of the parameter "*c*" is the same as what we have seen for the parameter "*b*".

Figures show that dispersive parameter "*b*" decreases when $\mu$ is increased while $\alpha$ and $\sigma_l$ are fixed. On the other hand "*b*" increases with an increasing non-thermal parameter $\alpha$ when other parameters ermine unchanged. But for high density situations which 0.6 < $\mu$ < 1 "*b*" approximately is independent of $\alpha$. Thus the width of soliton increases when $\alpha$ increases.

Eq. (15) has solitonic solutions and one-soliton solution for this equation is given by [16]

$$\phi_1 = \phi_m \sec h^2 \frac{\chi}{w} \tag{17}$$

where $\chi = \xi + \eta - u\tau$ and solition amplitude and width are

$$\phi_m = \frac{3(u-c)}{a} \qquad w = 2\sqrt{\frac{b}{u-c}} \tag{18}$$

Figures 3 show the soliton profiles with different values for the parameters. We can see that both compressive and rarefactive kinds can be created.

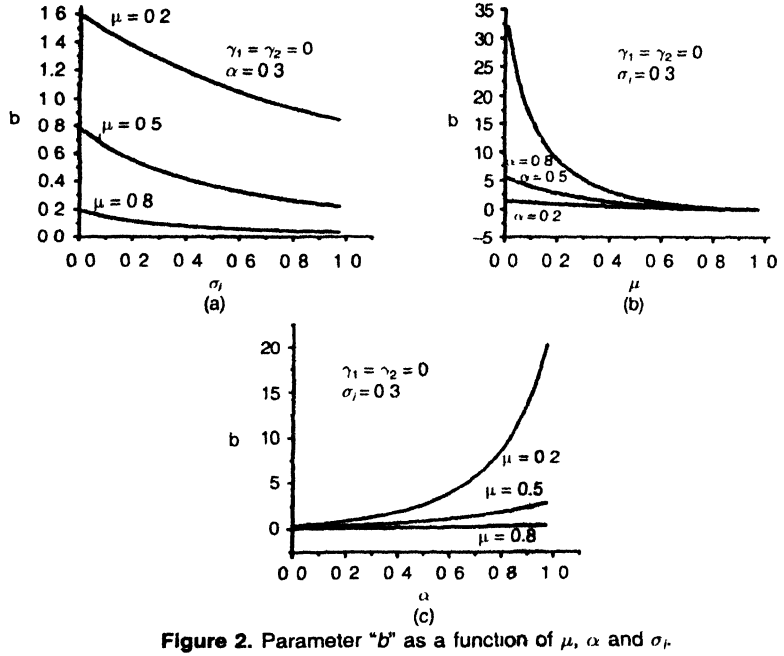


**Figure 2.** Parameter "*b*" as a function of $\mu$, $\alpha$ and $\sigma_i$.

The change of the type of the solition from rarefactive to compressive type is in agreement with the change of the parameter "*a*" with respect to medium parameters ($\alpha$, $\sigma_i$ and $\mu$). As an example, the $a$–$\alpha$ curve in Figure 1 shows that for $\mu$ = 0.5 and $0 < \alpha < 0.43$ the parameter "*a*" is negative. Thus we have rarefactive soliton in this region of parameters. Also for $a > 0.43$ "*a*" is positive and we expect to have compressive soliton. The $\phi$–$\chi$ plots with different values of $\alpha$ in Figure 3 are in agreement with the results of Figures 1.

## 4. The modified KP equation

The strength of the non-linear term in KP equation depends on the value of parameter

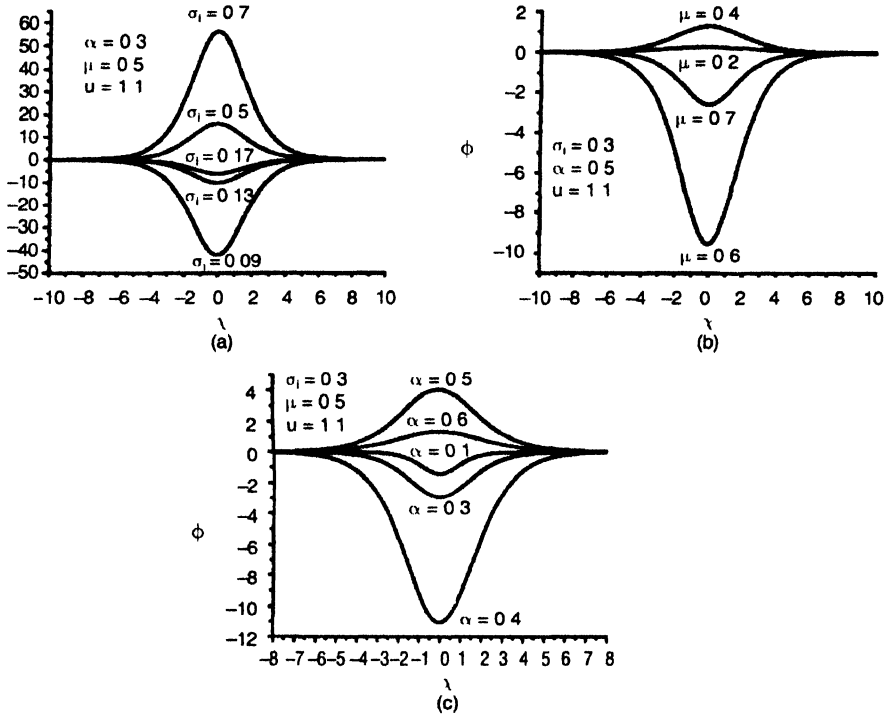


**Figure 3.** The soliton profiles of the KP equation for different values of parameter $\gamma_1$ and $\gamma_2$ are zero in all plots

"$a$" which is a function of $\mu$, $\beta$, $\sigma_I$, $\gamma_1$ and $\gamma_2$. The dependency of "$a$" can be studied by plotting this quantity as a fucntion of other parameters. By taking a specific value for the density (which is called critical density) it is possible that "$a$" becomes zero and thus $\phi_m$ increases to infinity. With the $\gamma_1 = \gamma_2 = 0$ the critical density is

$$\mu_c = \frac{6\sigma_I(1-\beta)+1+\sigma_I^2 \pm \left\{\left[6\sigma_I(1-\beta)+1+\sigma_I^2\right]^2 - 8\sigma_I^2\left(2+3\beta^2-6\beta\right)\right\}^{1/2}}{4\sigma_I^2} \quad (19)$$

In this case the stretching coordinate transformation is not valid. But we can save the equations by using a new set of parameters as follows

$$n_d = 1+\varepsilon n_{1d}+\varepsilon^2 n_{2d}+\varepsilon^3 n_{3d}+\ldots$$

$$u_d = \varepsilon u_{1d}+\varepsilon^2 u_{2d}+\varepsilon^3 u_{3d}+\ldots$$

$$v_d = \varepsilon^2 v_{1d}+\varepsilon^3 v_{2d}+\varepsilon^4 v_{3d}+\ldots$$

$$\phi = \varepsilon\phi_1+\varepsilon^2\phi_2+\varepsilon^3\phi_3+\ldots$$

$$Z_d = 1+\varepsilon^2\gamma_1\phi_1+\varepsilon^4\left(\gamma_1\phi_2+\gamma_2\phi_1\right)+\varepsilon^6\left(\gamma_1\phi_3+2\gamma_2\phi_1\phi_2+\gamma_3\phi_1^3\right). \quad (20)$$

Again by using (20) in the main eqs. (1) and collecting terms with the same powers of expanding parameters $\varepsilon$ we find eq. (14) for the lowest order. But for higher orders

of $\varepsilon$ we will have

$$n_{2d} = \frac{1}{2\lambda^2}\left(\frac{3}{\lambda^2} - \gamma_1\right)\phi_1^2, \quad u_{2d} = \frac{1}{2\lambda}\left(\frac{1}{\lambda^2} - \gamma_1\right)\phi_1^2 - \frac{\phi_2}{\lambda}$$

$$\frac{1}{\lambda^2} = \gamma_1 + \frac{\mu\sigma_i + 1 - \beta}{1-\mu} \tag{21}$$

$$\frac{\partial n_{1d}}{\partial \tau} - \lambda\frac{\partial n_{3d}}{\partial \xi} + \frac{\partial}{\partial \xi}\left(n_{1d}n_{2d} + n_{2d}u_{1d} + u_{3d}\right)\frac{\partial v_{1d}}{\partial \eta} = 0$$

$$\frac{\partial u_{1d}}{\partial \tau} + \frac{\partial}{\partial \xi}\left(u_{1d}u_{2d}\right) - \lambda\frac{\partial u_{3d}}{\partial \xi} = \frac{\partial \phi_3}{\partial \xi} + \gamma_1\frac{\partial}{\partial \xi}(\phi_1\phi_2) + \frac{\gamma_2}{3}\frac{\partial}{\partial \xi}(\phi_1^3)$$

$$\frac{\partial^2 \phi_1}{\partial \xi^2} = n_1 Z_2 + n_2 Z_1 + n_3 + Z_3 + \frac{\mu\sigma_i + 1 - \beta}{1-\mu}\phi_3 + \frac{1}{6}\left(\frac{\mu\sigma_i^3 + 1 - 3\beta}{1-\mu}\right)\phi_1^3 + \frac{\mu\sigma_i^2 - 1}{2(1-\mu)}\phi_1\phi_2$$

and

$$-\lambda\frac{\partial v_1}{\partial \xi} = \frac{\partial \phi_1}{\partial \eta}.$$

Finally, we have the following equation

$$\frac{\partial}{\partial \xi}\left[\frac{\partial \phi_1}{\partial \tau} + A\phi_1^2\frac{\partial \phi_1}{\partial \xi} + E\frac{\partial}{\partial \xi}(\phi_1\phi_2) + B\frac{\partial^3 \phi_1}{\partial \xi^3}\right] + C\frac{\partial^2 \phi_1}{\partial \eta^2} = 0 \tag{22}$$

where $A$, $E$, $B$ and $C$ are

$$A = \frac{1}{2}\left(\frac{4}{3}\gamma_2 + \frac{\gamma_1^2}{2}\right)\left[\gamma_1 + \frac{\mu\sigma_i + 1 - \beta}{1-\mu}\right]^{-1/2} - \frac{1}{2}\left[\gamma_3 + \frac{\mu\sigma_i^3 + 1 - 3\beta}{2(1-\mu)}\right]\left[\gamma_1 + \frac{\mu\sigma_i + 1 - \beta}{1-\mu}\right]^{-3/2}$$

$$+ \frac{15}{4}\left[\gamma_1 + \frac{\mu\sigma_i + 1 - \beta}{1-\mu}\right]^{3/2} - \gamma_1\left[\gamma_1 + \frac{\mu\sigma_i + 1 - \beta}{1-\mu}\right]^{1/2},$$

$$B = \frac{1}{2}\left[\gamma_1 + \frac{\mu\sigma_i + 1 - \beta}{1-\mu}\right]^{-3/2}, \quad C = \frac{1}{2}\left[\gamma_1 + \frac{\mu\sigma_i + 1 - \beta}{1-\mu}\right]^{-1/2}$$

$$E = -\left[\gamma_2 + \frac{\mu\sigma_i^2 - 1}{2(1-\mu)}\right]\left[\gamma_1 + \frac{\mu\sigma_i + 1 - \beta}{1-\mu}\right]^{-3/2}$$

$$+ 3\gamma_1\left[\gamma_1 + \frac{\mu\sigma_i + 1 - \beta}{1-\mu}\right]^{-1/2} - \frac{3}{2}\left[\gamma_1 + \frac{\mu\sigma_i + 1 - \beta}{1-\mu}\right]^{1/2}. \tag{23}$$

For critical density ($\mu_c$) "$E$" becomes zero and in this situation (22) reduces to the modified KP equation,

$$\frac{\partial}{\partial \xi}\left(\frac{\partial \phi_1}{\partial \tau}+A\phi_1^2\frac{\partial \phi_1}{\partial \xi}+B\frac{\partial^3 \phi_1}{\partial \xi^3}\right)+C\frac{\partial^2 \phi_1}{\partial \eta^2}=0\,. \tag{24}$$

This equation has solitonic solutions. One soliton solution for this equation is [11,18]

$$\phi_1=\pm\phi_m \operatorname{sec} h\left[(\xi+\eta-u\tau)/W\right] \tag{25}$$

where $u$, $\phi_m=\sqrt{6(u-C)/A}$ and $W=\sqrt{B/(u-C)}$ are velocity, amplitude and width of solitary wave respectively. The above results for one dimensional propagation with $\gamma_1$ =

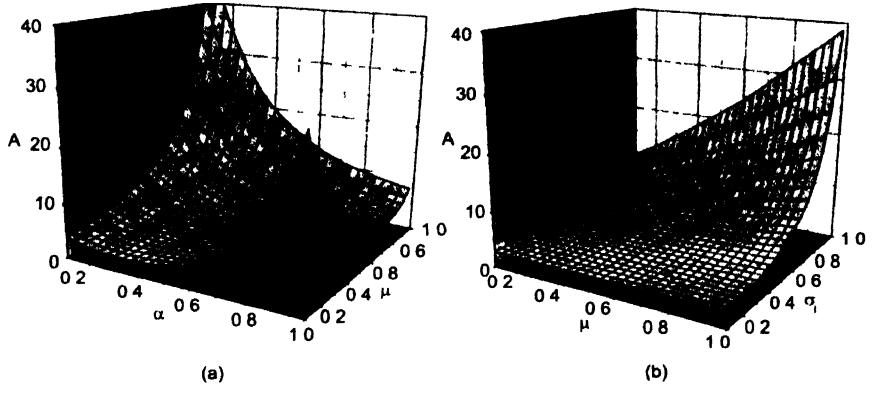


**Figure 4.** Parameter "$A$" as a function of $\mu$, $\alpha$ and $\sigma_i$ (a) $\sigma_i$=0 3 and (b) $\alpha$ = 0.3. In Figures $\gamma_1$, $\gamma_2$ and $\gamma_3$ are zero

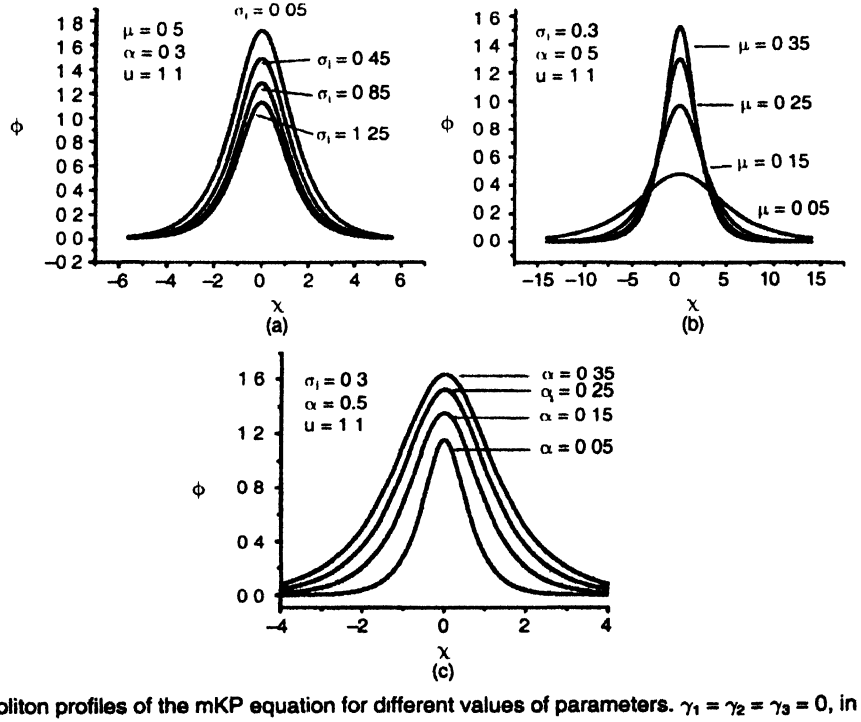


**Figure 5.** Soliton profiles of the mKP equation for different values of parameters. $\gamma_1 = \gamma_2 = \gamma_3 = 0$, in all the cases

$\gamma_2 = \gamma_3 = 0$ can be compared with results of reference [9]. Figures 4 show the coefficient "*A*" as functions of $\mu$, $\alpha$ and $\sigma_i$. The $\gamma_1$, $\gamma_2$ and $\gamma_3$ are all equal to zero in these Figures. It is clear that "*A*" is always positive.

Figures 5 show the soliton profiles with different values of the plasma parameters.

## 5. Conclusion

We studied small amplitude dust acoustic waves in dusty plasmas. We found the KP equation for a system of dusty plasma which contains Boltzmann distributed electrons and negative and variable charge of dust particles. The results which are presented in this section can be compared with what has appeared in [9] for the same system but with fixed charge for the dust particles and the results of [15] for warm plasma with the external static magnetic field. Also, the mentioned equations agree with those in reference [16].

Varying the amount of dust charge changes the strength of non-linear (parameter "*a*") and dispersive (parameter "*b*") terms [10,16,14,15]. A solitonic solution for the KP equation can not be found when the parameter "*a*" becomes zero. But in this case the KP equation changes to modified type of the KP equation. The mKP equation has stable solitonic solutions while the KP equation does not have any such solution for $a = 0$. The effects of non-thermal ions, density ($\mu$) and temperature ($\sigma_i$) on the behaviour of the solitions have been discussed by numerical simulations.

### References


[1] J H Chu, J B Du and I Lin *J. Phys.* **D27** 296 (1994)

[2] Q Z Luo, Anjelo and Merlino *Physics of Plasma* **6** 3455 (1999)

[3] A Barkan, N D'Angelo and R L Merlino *Planetary and Space Science* **44** 239 (1996)

[4] M R Gupta, S Sarkar, S Ghosh, M Debnath and M Khan *Physical Review* **E63** 046406 (2001)

[5] S Ghosh, S Sarkar, M Khan, K Avinash and M R Gupta *Physics of Plasma* **10** 977 (2003)

[6] S Ghosh, T K Chaudhuri, S Sarkar, M Khan and M R Gupta *Physical Review* **E65** 037401 (2002)

[7] S Ghosh, T K Chaudhuri, S Sarkar, M Khan and M R Gupta *Astrophys. and Space Sci.* **278** 463 (2001)

[8] T K Chaudhuri, M Khan and M R Gupta *Physics of Plasma* **14** 463 (2007)

[9] M M Lin and W S Duan *Chaos, Solitons & Fractalse* **33** 1189 (2007)

[10] W S Duan *Chaos Soliton. Fract.* **14** 503 (2002)

[11] Z X Wang, X Wang, L W Ren, J-Y Liu and Yue Liu *Phy. Lett.* **A339** 96 (2005)

[12] Z X Wang, X Wang, L W Ren, J-Y Liu and Yue Liu *Phy. Lett.* **A347** 264 (2005)

[13] Y Y Wang and J F Zhang *Phys. Lett.* **A352** 155 (2006)

[14] W S Duan, X R Hong, Y R Shi and J A Sun *Chaos Soliton. Fract.* **16** 767 (2003)

[15] L P Zhang and J K Xue *Chaos Soliton. Fract.* **23** 543 (2005)

[16] T S Gill, S S Nareshpal and K Harvinder *Chaos Soliton. Fract.* **28** 1106 (2006)

[17] S Ghosh, Bharuthram, M Khan and M R Gupta *Physics of Plasma* **11** 3602 (2004)

[18] M Wadati *J. Phys. Soc. Jpn.* **34** 1289 (1973)

*Indian J. Phys.* **82 (12)** 1701-1705 (2008)

*Note*

IJP

# Surface stress calculation for one-monolayer adsorption of As on the Si(001) and the Ge(001) surfaces

J D Dubey[1]*, J P Kushwaha[2] and Bhimlal Prasad[1]

[1]Department of Physics, Vinobha Bhave University, Hazaribag-825 301, Jharkhand, India

[2]J P College, Narayanpur, Tilka Manjhi Bhagalpur University, Bhagalpur-853 203, Bihar, India

E-mail : jd_dube2004@yahoo.co.in

*Received 12 February 2008, accepted 8 May 2008*

**Abstract** : We report a surface stress calculation for one-monolayer adsorption of As on the Si(001) and the Ge(001) surfaces. The density functional theory within local density approximation has been used. A comparison of our two results show that the As-adsorbed-Ge surface is more isotropic than the As-adsorbed-Si surface. The adsorption of As removes the original Si (Ge) asymmetric dimers and forms symmetric dimers. This is attributed to the decrease in stress anisotropy due to the introduction of defects on the surface. This inference is in agreement with that of He and Zhang who studied a Sb-adsorbed-Si(001) surface.

**Keywords** : Surface stress, adsorption, arsenic, germanium, silicon, density functional theory, stress anisotropy.

**PACS Nos.** : 73.20.-r, 73.20.At, 73.20.Hb

The adsorption of group-V elements on the surfaces of group-IV elements has been the subject of great interest both theoretically and experimentally in the last few years. The interest has grown because of the influence of group-V elements in enhancing the abruptness of the interface in crystal growth of heterostructures by acting as surfactants, and in modifying the electronic properties by acting as dopants [1]. The adsorption of As, under good experimental conditions leads to a well ordered symmetric dimer structure on both Si(001) and Ge(001) structure [2,3]. Arsenic lowers the surface free energy of both Ge and Si, and it can be used as surfactant in the growth of Si on Ge(001) [4]. The surface stress has been recognized to play important role in the adsorption process of As on Si(001) and Ge(001) surfaces [5,6]. In this paper we report our study of the surface stress calculation of 1-mono-layer adsorption of As on the

*Corresponding Author

Si(001) and Ge(001) surfaces employing an *ab initio* pseudopotential method.

In this study we have used the density functional theory of Hohenberg, Kohn and Sham (HKS) [7–9] with the utility of the ABINIT code which in based on pseudopotential and plane waves [10]. The electron-ion interaction was included in the form of norm-conserving pseudopotential [11] that are fully separable in the Kleinman-Bylander form [12]. The pseudopotentials were generated using the FHI98pp code [13]. The electron-electron interaction was considered within the local density approximation using the correlation scheme of Perdew and Wang [14].

A brief outline of the density functional theory is given below.

This theory puts charge density at the centre stage. The solution of Schrödinger equation in an external potential would result in a certain ground state wave function $\Psi$ to which is associated a certain charge density

$$\rho(r_1) = \sum M \int |\Psi(x_1, x_2 \ldots\ldots\ldots x_m| \, dx_1, dx_2 \ldots\ldots\ldots dx_m) . \tag{1}$$

Further, there is a certain energy functional which is minimized by the unknown ground charge density, $\rho$. The Kohn-Sham energy functional is formally written in the form

$$H_{ks} = \hbar^2/2m \cdot \nabla^2 + V_{eff} \tag{2}$$

where the effective potential is defined as for a one-electron potential

$$V_{eff} = V_N(\rho) + V_H(\rho) + V_{XC}(\rho) \tag{3}$$

The energy term associated with the nuclei-electron interaction is $\langle V_N \mid \rho \rangle$ while that associated with the electron-electron interaction is $\langle V_H \mid \rho \rangle$ where $V_H$ is Hartree potential.

$$V_H = \int \rho(r')/|r - r'| \cdot dr' . \tag{4}$$

The Kohn-Sham energy functional is written as

$$E(\rho) = (-\hbar^2/2m) \sum_{i=1}^{N} \int \Phi_i^*(r) \nabla^2 \Phi_i(r) dr + \int \rho(r) V_{ion}(r) dr$$

$$+ 1/2 \iint \rho(r)\rho(r')/|r - r'| \cdot dr dr' + E_x \{\rho(r)\} . \tag{5}$$

Within local density approximation the exchange energy is expressed as

$$E_x \{\rho(r)\} = \int \rho(r) \sum\nolimits_x [\rho(r)] \, d^3r \tag{6}$$

where $E_x$ $[\rho(r)]$ is the exchange energy per particle of a uniform gas at a density of $\rho$. The exchange potential can be determined from the functional derivative of $E_x[\rho(r)]$

$$i.e.\ V_x(\rho) = \delta E_x(\rho)/\delta\rho . \tag{7}$$

Using Hartree-Fock theory it has been shown that the exchange energy of a free

electron gas is given by

$$E_{HF}^{FEG} = 2\sum_{K<Kf} \hbar^2 k^2/2m$$

$$-(e^2 k_f/\pi)\sum_{K<Kf}\left[1+\left\{\left\{1-(k/k_f)^2\right\}/2(k/k_f)\right\}\ln\left|(k+k_f)/(k-k_f)\right|\right. . \tag{8}$$

Comparing with HF expression for the exchange energy of a 'free electron gas' one obtains for the potential

$$V_x(\rho) = -(e^2/\pi)\cdot\left\{3\pi^2\rho(r)\right\}^{1/3} . \tag{9}$$

Correlation energies can be included in the energy functional, having the form in LDA

$$V_{xc}\left\{\rho(r)\right\} = V_x\left\{\rho(r)\right\} + V_c\left\{\rho(r)\right\} \tag{10}$$

where $V_c$ represents the contribution to the total energy beyond HF limit. Spin is included as

$$\rho = \rho\uparrow + \rho\downarrow$$

where $\uparrow$ and $\downarrow$ represents 'up' and 'down' spins.

The Kohn-Sham equation for the electronic structure of matter is given by

$$\left(-h^2\nabla^2/2m + V_N(r) + V_H(r) + V_{XC}\left[\rho(r)\right]\right)\Phi_i(r) = E_i\Phi_i(r) . \tag{11}$$

The KS equation is solved in LDA by using pseudopotential. The pseudopotential model treats matter as a sea of valence electrons moving in a background of ion cores composed of nuclei and inert inner electrons.

The KS equation must be 'discretized' *i.e.* be reduced from a virtually infinite-unknown problem to a finite-unknown problem. For crystals, plane wave basis has been quite effective.

The plane wave used is of the following form.

$$\Psi_k(r) = \sum_G \alpha(\boldsymbol{k}.\boldsymbol{G})\exp(i/\left|\boldsymbol{k}+\boldsymbol{G}\right|\cdot\boldsymbol{r}) \tag{12}$$

where $\boldsymbol{k}$ = wave vector and it is a quantum number represented as $k = k_1, k_2, k_3$,

$\boldsymbol{G}$ = reciprocal lattice vector and

$\alpha$ $(\boldsymbol{k}.\boldsymbol{G})$ = co-efficient of basis.

When expressed in a plane wave basis, the Hamiltonian is actually dense matrix. Specifically, the Laplacian term of the Hamiltonian is represented by diagonal matrix and the potential term gives rise to a dense matrix.

For non-periodic systems the plane wave basis is combined with a 'super cell' method. The super cell repeats the localized configuration to impose periodicity to the systems. This preserves the "artificial" validity of $\boldsymbol{k}$ and Bloch's theorem which eq. (12) obeys.

For the surface stress calculations we considered a symmetrical unit cell which included an atomic slab with five layers of Ge(Si) and mono-layer of As on each surface. The vacuum region between slabs was taken to be about five mono-layers in thickness. All of the atoms were allowed to relax except the two Ge(Si) layers in the middle of the slab. This choice of slab thickness was found to be adequate as the main contribution to the surface stress come from the first three atomic layers. Single particle wave functions were expanded with a plane wave basis upto a kinetic energy cut off of 12 Ry. The integration in the Brillouin Zone was performed using 8 special $k$ points sampled within the Monkhorst pack scheme [15].

We considered three adsorption sites for the adsorbate As atom : (a) the non-diffused configuration, (b) 50% inter diffusion of As into the 2nd substrate layer and (c) 100% interdiffusion of As into the 2nd substrate layer *i.e.* As-atomic-layer replacing the top Ge(Si) atomic layer. The calculated bond lengths are : As-As $\approx$ 0.252 nm, As-Ge $\approx$ 0.250 nm, Ge-Ge $\approx$ 0.244 nm, As-Si $\approx$ 0.247 nm, Si-Si $\approx$ 0.250 nm.

For computing the surface stress for each of the three As adsorbed surface geometries the following three dimensional stress tensor expression was employed.

$$g_{\alpha\beta} - (C/2)\cdot\sigma_{\alpha\beta}^{\text{corr}} = (C/2)(\sigma_{\alpha\beta} + \chi\delta_{\alpha\beta}) \tag{13}$$

where $C$ is the height of the supercell, $\chi$ is the finite basis correction, and $\sigma_{\alpha\beta}$ the three dimensional supercell stress tensor. The results of the present calculation are given in the Table 1. These result show that the lowest energy configuration of (a) is characterized by stress which is compressive along the surface dimer row direction and tensile in the orthogonal direction. A comparison of our two results show that the As-adsorbed-Ge surface is more isotropic than the Si-adsorbed-Ge surface. The total-energy minimization calculations show asymmetric dimers for Si(001) and Ge(001). The adsorption of As removes the original Si(Ge)-dimer reconstruction and forms symmetric dimers [16,17]. This is attributed to the decrease in stress anisotropy due to the introduction of defects on the surface. This inference is in agreement with that of He *et al* [18] who studied a Sb-adsorbed-Si(001) surface.

**Table 1.** Calculated surface stress in (eV/(1 x 1) unitcell), for direction both perpendicular ($g\perp$) and parallel ($g_{\|}$) to dimer. The differences ($g_{\|} - g\perp$) represent the stress anisotropy.

| | As/Si | | | | As/Ge | | |
|---|---|---|---|---|---|---|---|
| | ($g\perp$) | ($g_{\|}$) | ($g_{\|} - g\perp$) | | ($g\perp$) | ($g_{\|}$) | ($g_{\|} - g\perp$) |
| As-capped (a) | –0.59 | 0.67 | 1.26 | As-capped (a) | –0.38 | 0.75 | 1.13 |
| 2nd layer (b) | –0.85 | 0.34 | 1.19 | 2nd layer (b) | –0.47 | 0.32 | 0.79 |
| Si-capped (c) | –0.92 | –0.15 | 0.77 | Ge-capped (c) | –0.61 | –0.09 | 0.52 |

## Acknowledgment

A part of this work was financially supported by the University Grants Commission of

India in the form a Minor Research Project granted to JPK. We also thank the Universite' Catholique de Louvain, Corning Inc., for the ABINIT code.

**References**

[1] L H Chan and E I Altman *Phys. Rev.* **B63** 195309 (2001)

[2] P Krüger and L Pollman *Appl. Phys.* **A59** 487 (1994)

[3] J F Morar, U O Karlsson, R I G Uhrberg, J Kanski, P O Nilsson and H Qu *App. Surf Sc.* **41/42** 312 (1980)

[4] M Copel, M C Reuter, M V Hoegen and R M Tromp *Phys. Rev.* **B42** 11682 (1990)

[5] R M Tromp, A W Denier van der Gon and M C Reuter *Phys. Rev. Lett.* **68** 2313 (1992)

[6] R M Tromp *Phys. Rev.* **B47** 7125 (1993)

[7] P Hohenberg and W *Kohn Phys. Rev.* **B136** 864 (1964)

[8] W Kohn and L J Sham *Phys. Rev.* **A140** 1133 (1965)

[9] R M Dreizler and E K U Gross *Density Functional Theory* (Berlin Springer-Verlag : Heidelberg) (1990)

[10] J Nogami, A A Baski and C F Quale *Appl. Phys. Lett.* **58** 475 (1991)

[11] D R Hamann *Phys. Rev.* **B40** 2980 (1989)

[12] L Kleinman and D M Bylander *Phys. Rev. Lett.* **48** 1425 (1982)

[13] M Fuchs and M Scheffler *Comp. Phys. Commun.* **119** 67(1999)

[14] J P Perdew and Y Wang *Phys. Rev.* **B45** 13244 (1992)

[15] H J Monkhorst and J D Pack *Phys. Rev.* **B13** 5188 (1976)

[16] John P LaFemina *Surface Science Reports* **16** 133 (1992)

[17] M E Gonzalez-Mendezand Takeuchi *Bhys. Sat. Sol.* **B220** 79 (2000)

[18] Yao He, X H Zhang and J G Che *Phys. Rev.* **B66** (2002)

*Indian J. Phys.* **82** (12), 1707 (2008)

# FORTHCOMING PUBLICATIONS

## Volume 83 (2009)

### *Special Issue on "Simulation Physics – New Strategies and Applications"*

Forword

***Invited Articles***

*Ab initio* molecular dynamics investigations of structural, electronic and dynamical properties of water in supercritical carbon dioxide

MOUMITA SAHARAY AND SUNDARAM BALASUBRAMANIAN

How does contrasting dependence of impurity-atom diffusivity on the density of host disordered medium arise?

MANJU SHARMA AND S YASHONATH

Effect of unfolding on the thickness of the hydration layer of a protein

SUDIPTA KUMAR SINHA, SUDIP CHAKRABORTY AND SANJOY BANDYOPADHYAY

Relationship between crystalline order and melting mechanisms of solids

SOMENDRA NATH CHAKRABORTY, SURMA TALAPATRA AND CHARUSITA CHAKRAVARTY

Molecular dynamics simulation of HIV – protease with polarizable and non-polarizable force fields

B R MEHER, M V SATISH KUMAR AND PRADIPTA BANDYOPADHYAY

Pressure effects on diffusion in liquid ammonia : A simulation study using a combination of isobaric-isothermal and microcannonical molecule dynamics

SNEHASIS CHOWDHURI, DEBASHREE CHAKRABORTY AND AMALENDU CHANDRA

*Indian J. Phys.* **82 (12)**, 1709-1712 (2008)

# NOTES FOR CONTRIBUTORS

INDIAN JOURNAL of PHYSICS

## 1. Publications Scheme

Indian Journal of Physics is published monthly, containing 12 regular issues in a year, from January to December.

## 2. Scope

Astrophysics, Atmospheric & Space Physics / Atomic & Molecular Physics / Biophysics / Condensed Matter & Material Physics / General & Interdisciplinary Physics / Nonlinear Dynamics & Complex Systems / Nuclear Physics / Optics & Spectroscopy / Particle Physics / Plasma Physics / Relativity & Cosmology / Statistical Physics

## 3. Refereeing

All contributions submitted are refereed. The Board of Editors reserve the right to reject manuscript and to edit a contribution whenever / wherever necessary.

## 4. Publication Speed

Normally the contributions are published within six months of the acceptance. In order to keep delays to a minimum, it is of utter importance for the authors to follow '**Preparation of Manuscripts**' (see below) strictly, before submission of the manuscript. Also the revised version (in the light of referee's comments) of the paper should be returned **within a fortnight of the date of receipt**. 'Rapid communications' are published within 3 months of the date of acceptance.

## 5. Preparation and Submission of Manuscripts

The followings are the requirements which should be met before submission of the manuscripts to Indian Journal of Physics.

### (i) Manuscript

The original typescript for a **full paper** should be typed on one side of good quality bond paper, with double spacing and a wide margin (Single Column, print **area** - 21 cms × 15 cms). The title page should contain title, author(s), address(es), abstract, PACS Nos. **and** Keywords. The main text should start on a new page. All pages should be numbered. The paper **must** be divided into sections starting preferably with 'Introduction' and ending with 'Conclusions'. The **main** sections should be numbered as 1, 2, 3, *etc.* and the subsections as 2.1, 2.2, 2.3 *etc.*

**Rapid communication** is devoted to the announcement of timely and important results. Contributions to this and **Note** sections should not exceed 8 typed pages (double spaced), including figures, equations, tables and references. They should follow the same style and format as the full paper except that they need not be divided into sections.

The **Review Article** in frontier topics must be prepared as per format of the full paper. Such article should have a coverage of 25-50 printed pages of the journal. Three copies of the extended abstract along with a plan of the article and short bio-data of the reviewers, must be sent prior to the communication of the review article.

Manuscripts of the **Proceeding** may be submitted (after being refereed and properly edited by the Convener/Guest Editor) in a Camera-ready format in a CD. A prior approval from the Board of Editors is, however, required for its publication.

Net amount charged for publication of Proceeding of 100 pages (or part thereof) is Rs 20,000 00 only which includes free copies to the participants (not exceeding 100)

**Manuscript in triplicate, of which one is a clear master copy with original figures, should be sent to the *Assistant Registrar –I Mr. S Sahoo, Indian Journal of Physics* with a mention of the field under which the paper is being submitted and a list of potential referees in that area / field.**

**Manuscript may also be submitted through an appropriate member of the Board of Editors. In that case, one copy of the manuscript is to be sent to the member concerned and two other copies must be submitted to the Editorial Office with an intimation.**

**Final version of the Manuscript (after being accepted and edited) must be submitted in a CD (containing the Text in MSWORD / La Tex, and the Figures in Post Script Files) before it is scheduled for publication. No article will be published without CD.**

**(ii) Title**

The title should be brief and yet convey to the informed reader the particular nature of the contents of the paper

**(iii) Address**

The Name(s) of the author(s) and address(es) of the institute where the research work was done, should be indicated The name of the author to whom correspondence is to be addressed, should be underlined The present address(es) of the author(s), if it is different, may be given as a *foot note* E-mail address of the corresponding author must be provided

**(iv) Abstract**

An abstract of less than 200 words is required It should contain the essence of the result achieved

**(v) Keywords and PACS numbers**

Appropriate **Keywords** and **PACS Nos** (*Physics and Astronomy Classification Scheme of American Institute of Physics*) (not more than six) must be provided for indexing and information retrieval services PACS is available online (http //www aip org/pacs/)

**(vi) Text**

In the preparation of text, the authors should pay attention to the language (usage of words grammar and construction of sentences), logical presentation, enumeration of assumptions made, justifications of approximations made *etc* and all the limitations must be stated whenever and wherever necessary Moreover, a paper must be self-contained, its presentation being clear, concise and satisfactory

**(vii) Figures**

The number of figures should be kept to the minimum Each figure must be referred to in the text, be numbered and have a caption The captions should be typed on a separate sheet The appropriate place of the figure should be indicated in the margin of the text Axes of figures must be labelled properly The letterings as well as the essential details be inserted in all the submitted copies Waste space at the top and bottom should be avoided After acceptance, electronic files for the figures (Post Script Files) are to be submitted in a CD.

**(viii) Tables**

Tables should be typed on separate sheets and each table should have a number and a self-explanatory title Column headings of tables should be brief Footnotes to the tables, if any, should be identified by superscript letters and placed at the bottom of the table. When papers include extensive tabular material or appendices, which may be of interest to relatively few readers, the material should be deposited with the Editorial Office

**(ix) Formulae**

Displayed formula should be numbered, typed or written by hand clearly and unambiguously Vectors, special symbols, superscript and subscripts *etc* should be identified with proper signs in the manuscript Long equations should be avoided as much as possible, by introduction of suitable abbreviations of component expressions The exp' form of complex exponential functions [**Exp (–*kr*) instead of** $e^{-kr}$], fractional exponents instead of root signs [$x^{y_2}$ **instead of** $\sqrt{x}$] and solidus (/) for fractions [*a*/*b* **instead of** $\frac{a}{b}$] are preferable International conventions in the choice of symbols, units and notations should be followed

**(x) References**

All references referred to text tables and figures of a manuscript must be combined in a single list, numbered consecutively in their order of first appearance and arranged in the same order at the end of the text material They should be cited in text by Arabic numerals in square brackets at appropriate places of a sentence, for example [1-5] *etc* The references cited should be limited to the absolute minimum and the list to be submitted in a separate sheet containing names of all authors (*et al*' is not allowed) They should be as complete as possible and be presented as follows

[6] U Fano and A R P Rao *Atomic Collisions and Spectra* (New York Academic) **Vol 1**, Ch 2, Sec 4, p 25 (1986)

[7] T Atsumi T Isihara, M Koyama and M Matsuzawa *Phys Rev* **A42** 6391 (1990)

[11] T Le-Brun, M Lavollee and P Morin *X ray and Inner Shell Processes* (AIP Conf Proc 215) (eds) T A Carlson, M O Krause and S Manson (New York AIP) p 846 (1990)

[14] S B Hansen, K B MacAdam and L G Gray *12th Int Conf on Atomic Physics* (Ann Arbor) Abstracts px-12 (1990)

[15] H Pauly *Atomic and Molecular Beams Methods* (eds) G Scoles, D Bassi, U Buck and D Laine (London Oxford University Press) p 83 (1988)

[19] W Fritsch (private communication) (1988)

[21] K B MacAdam (to be published) (1991)

[23] I Roy *PhD Thesis* (University of Calcutta, India) (1992)

**(xi) Footnotes**

As far as possible, footnotes should be avoided

**(xii) Appendices**

All appendices should be numbered consecutively and typed on separate sheets

**Manuscripts which do not conform to these conventions are returned to the authors immediately.**

**6. Reprints**

A reprint order form sent to the corresponding author must be returned to ***the Staff Editor (Technical Officer-II) Mr A N Ghatak,*** *Indian Journal of Physics Indian Association for the Cultivation of Science, Jadavpur, Kolkata 700 032, India (e mail adhirnath@gmail com)* **within two days from the date of receipt** There is no page charge **A Complimentary copy of the Journal and 10 (ten) copies of the reprints will be sent to the Corresponding Author, free of charge** However, extra copies of reprints (with/without cover) may be ordered with remittance in advance (along with reprint order and signed copyright Form) at the following revised rates (from January 2000 onwards)

| | | |
|---|---|---|
| Page | Foreign | US $ 20 00 per page per 50 copies or part thereof |
| | Inland | Rs 150 00 per page per 50 copies or part thereof |
| Cover | Foreign | US $ 30 00 per cover of 50 copies or part thereof |
| | Inland | Rs 250 00 per cover of 50 copies or part thereof |
| Art Plate | Foreign | US $ 30 00 per page/colour of 50 copies or part thereof |
| | Inland | Rs 250 00 per page/colour or 50 copies or part thereof. |

**If the reprint order is not received in time, later request for any more reprints cannot be complied with.**

**7. Corrections and Modifications**

Authors are requested to exercise utmost care in preparation of manuscripts so that there is little need to incorporate alterations at the Final stage Extensive modifications at this stage are not allowed

**8. Correspondence**

All correspondences regarding the manuscripts should be sent to the ***Assistant Registrar-1, S Sahoo*** *Indian Journal of Physics Indian Association for the Cultivation of Science, Jadavpur, Kolkata-700 032, India (e-mail ssahoo_ijp@yahoo com)* with full reference to the paper concerned *i e* the name(s) of author(s) the full title and the reference number (given by the Editorial Office)

## IMPORTANT INSTRUCTIONS TO THE CONTRIBUTORS

The authors are requested to include the following important Information in their Covering Letters submitting the papers to Indian Journal of Physics

*(i) The mailing address of the Corresponding Author with E mail, Fax and Phone Nos*

*(ii) A list of Potential Referees with postal and e-mail addresses for the submitted Manuscript*

*(iii) The specific Field under which the Manuscript is to be placed*

*(iv) Whether the Manuscript should be published as (a) Review (b) Full paper, (c) Short note, (d) Rapid communication*

*(v) Justification if the Manuscript is to be published as a Rapid Communication*

## SUBSCRIPTIONS

| | | |
|---|---|---|
| Periodicity | 12 issues per year (January–December) | |
| Foreign | Annual<br>US $ 500 00<br>(including air freight) | Single<br>US $ 50 00<br>(including air freight) |
| Inland | Rs 1,500 00 (including postage) | Rs 150 00 (including postage) |
| Discount | 25% (Agents/Book-Sellers)<br>50% (Research Scientists & Students for direct subscription)<br>Rs 500 00 (Annual subscription for IACS and IPS members only if subscription be received within December of the preceding year) | |

Demand draft (D/D) to be drawn on any bank at Kolkata Branch in favour of "***Indian Association for the Cultivation of Science***", and this along with other relevant enquiries should be sent to the ***Assistant Registrar–I***, *Indian Journal of Physics, Indian Association for the Cultivation of Science, Jadavpur, Kolkata-700 032, India* Out-station cheque may be accepted with an additional amount of **Rs. 75.00**, in addition to subscription rates of Rs 1,500 00

Journal will be supplied against advance payment only

**Phone** : (+91) (33) 2473-4971 (Extn 160,161,162,452)

**Gram** : Indasson, Jadavpur

**Fax** : (+91) (33) 2473 2805

**e-mail** : ijp@iacs.res in

**Web** : http://www.iacs res in/ijp html

*Indian J. Phys.* **82 (12)**, 1713-1714 (2008)

IJP

# r Special Publications

I *Commemorative Volumes to mark the celebration of 75th year of publication of Indian Journal of Physics Volumes 1–6

1 Frontiers in Materials Physics
Guest Editor D Chakravorty
Price Rs 600 00 (10 articles, 247 pages, illustrated)
Date of Publication 2002

2 Frontiers in Astrophysics
Guest Editor Sandip K Chakrabarti
Price Rs 600 00 (12 articles, 303 pages, illustrated)
Date of Publication 2002

3 Frontiers in Atomic, Molecular & Optical Physics
Guest Editors S S Bhattacharyya and S C Mukherjee
Price Rs 600 00 (15 articles, 429 pages, illustrated)
Date of Publication 2003

4 Frontiers in High Energy Physics
Guest Editors Amitava Raychaudhuri and Partha Mitra
Price Rs 600 00 (11 articles, 281 pages, illustrated)
Date of Publication 2004

5 Frontiers in Condensed Matter Physics
Guest Editors J K Bhattacharjee and B K Chakrabarti
Price Rs 600 00 (7 articles, 308 Pages, illustrated)
Date of Publication 2005

6 Frontiers in Biophysics
Guest Editors T P Singh and Chanchal Das Gupta
Price Rs 600 00 (12 articles, 188 pages, illustrated)
Date of Publication 2005

*For Volumes 1–6, please contact Publishers

**Messrs. Allied Publishers Pvt. Ltd.**
A-104, Mayapuri, Phase-II, New Delhi-110 064, India
17, Chittaranjan Avenue, Kolkata-700 072, India
15, J N. Heredia Marg, Ballard Estate, Mumbai-400 038, India
751, Anna Salai, Chennai-600 002, India

II. Landmark Papers in Indian Journal of Physics [1926–2001]
Guest Editors : J K Bhattacharjee and D S Ray
Price : Rs. 500.00; US $. 50.00 (289 pages, illustrated)
Date of Publication : December, 2002

III. 75th Year of Discovery of Raman Effect : A Special Issue of India Journal of Physics [1928–2003]
Guest Editor : S Chakravorti
Price : Rs. 500.00; US $. 50.00 (164 pages, illustrated)
Date of Publication : February, 2003

IV. Production of Radioactive Ion Beams [PRORIB–2001]
Proceedings of the DAE–BRNS sponsored International Workshop–A Special Issue of Indian Journal of Physics
Guest Editor : Alok Chakrabarti
Price : Rs. 200.00; US $. 50.00 (226 pages, illustrated)
Date of Publication : May, 2002

V. Commemoration Volume on Professor K S Krishnan :
Birth Centenary [1898–1998]
Guest Editors : S Ray and C K Majumdar
Price : Rs. 100.00; US $. 40.00 (332 pages, illustrated)
Date of Publication : December, 1999

VI. Physics and Technology of Accelerators : A Special Issue of Indian Journal of Physics on the occasion of Golden Jubilee of India's Independence
Guest Editor : Debashis Basu
Price : Rs. 100.00; US $. 40.00 (236 pages, illustrated)
Date of Publication : December, 1999

VII. Recent Trends in Statistical Physics : A Special Issue of
Indian Journal of Physics
Guest Editor : J K Bhattacharjee
Price : Rs. 100.00; US $. 40.00 (140 pages, illustrated)
Date of Publication : August, 1998

VIII. XI DAE Symposium of High Energy Physics : A Special
Issue of Indian Journal of Physics
Guest Editor : Ranabir Dutt and Asim K Ray
Price : Rs. 300.00; US $. 100.00 (395 pages, illustrated)
Date of Publication : February, 1997

IX. Lectures of Theoretical Physics Seminar Circuit [1990-92] : A Special Issue of Indian Journal of Physics
Guest Editors : C K Majumdar and Partha Ghosh
Price : Rs. 80.00; US $. 35.00 (100 pages, illustrated)
Date of Publication : November, 1993

X. Commemoration Volume on Professor Meghnad Saha : Birth Centenary [1893-1993]
Editors : H Banerjee and S P Sen Gupta
Price : Rs. 140.00; US $. 40.00 (240 pages, illustrated)
Date of Publication : December, 1993

XI. High Temperature Superconductivity Lectures of
Theoretical Physics Seminar Circuit [1989-90] : A Special Issue of Indian Journal of Physics
Editors : B K Chaudhuri and S P Sen Gupta
Price : Rs. 80.00; US $. 30.00 (220 pages, illustrated)
Date of Publication : March, 1992

XII. Commemoration Volume on Professor C V Raman :
Birth Centenary [1888–1988]
Editor : S P Sen Gupta
Price : Rs. 50.00; US $. 25.00 (225 pages, illustrated)
Date of Publication : July, 1989

**(Please contact us for all these Special Publications)**

*Indian J. Phys.* **82**, Index (Author & Subject), 1715-1747 (2008)

# INDIAN JOURNAL OF PHYSICS

**Volume 82**

AND

PROCEEDINGS OF THE

Indian Association for the Cultivation of Science, **Vol. 91**

## Author & Subject Index

**(2008)**

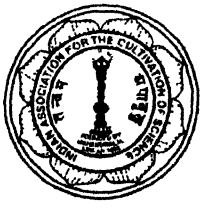


*(Published by the Indian Association for the Cultivation of Science in Editorial Collaboration with the Indian Physical Society)*

*Indian J. Phys.* **82**, Index / Author 1717-1731 (2008)

IJP

# INDIAN JOURNAL OF PHYSICS

## AUTHOR INDEX*

### VOLUME 82

### (2008)

The following *abbreviations* are used :

(*E*) *Erratum*

(*N*) *'Note'*

($P_1$) *Proceedings (Part I & II) of the National Symposium entitled Condensed Matter Days-2006 (CMDAYS-06) organised by the Department of Physics, Tezpur University, P.O.-Nappam, Tezpur-784 028, Assam, India held at Tezpur, India, during August 29-31, 2006*

($P_2$) *Proceedings (Part I & II) of the 5th Biennial Conference of the Physics Academy of the North East (PANE) held at Department of Physics, Gauhati University, Guwahati-781 014, Assam, India during March 1-2, 2007*

(*R*) *'Review'*

(*RC*) *'Rapid Communication'*

($S_1$) *Special Issue on 80 years of the Discovery of Raman Effect & 175th Birth Anniversary of Dr. Mahendra Lal Sircar*

($S_2$) *Special Issue on "Electrodynamics of Classical Charged Particles"*



*Indexed on the basis of the first author

*Indian J. Phys.* **82**, Index / Subject 1733-1747 (2008)

# INDIAN JOURNAL OF PHYSICS

## SUBJECT INDEX

### VOLUME 82

### (2008)

## *Atomic & Molecular Physics*



## *Condensed Matter & Material Physics*

## *General & Interdisciplinary Physics*

## *Nonlinear Dynamics & Complex Systems*



## *Nuclear Physics*



## *Optics & Spectroscopy*

## Particle Physics



## Plasma Physics



## Statistical Physics



## Notes

## *Proceedings (Part I & II) of the National Symposium entitled Condensed Matter Days-2006 (CMDAYS-06) organised by the Department of Physics, Tezpur University, P.O.-Nappam, Tezpur-784 028, Assam, India, held at Tezpur, India, during August 29-31, 2006*

## *Proceedings (Part I & II) of the 5th Biennial Conference of the Physics Academy of the North East (PANE) held at Department of Physics, Gauhati University, Guwahati-781 014, Assam, India during March 1-2, 2007*

### *Foreword*



### *Invited Talk*

***Reprinted from Indian Journal of Physics Vol. II and Proceedings of the Indian Association for the Cultivation of Science Vol. XI***

***Vol. II, Part III (24) pp 387-398 (1927-1928)***



## *The Discovery of the Raman Effect*



## *Special Issue on "Electrodynamics of Classical Charged Particles"*

## *Erratum*

*Indian J. Phys.* **82** (**12**), 1749 (2008)

# RENEWAL NOTICE 2009

## INDIAN ASSOCIATION FOR THE CULTIVATION OF SCIENCE

JADAVPUR, KOLKATA-700 032, INDIA

To All Subscribers of Indian Journal of Physics.

Your subscription, which expires with the despatch of December, 2008 issue of the journal, will stand for renewal. We request you to send the Renewal Order of Volume 83 (2009) at your earliest. The subscription rates for Volume 83 (2009) are mentioned below which we have been compelled to increase due to increasing the cost of Printing and stationary. Kindly mention your Subscription No. of 2008 while placing Renewal Order.

Please note that the supply of journal for Volume 83 (2009) will commence on receipt of subscription fee, in advance.

**S. Sahoo**
Assistant Registrar-I,
Indian Journal of Physics

## SUBSCRIPTION RATES : VOLUME 83 (2009)

### INDIAN JOURNAL OF PHYSICS

(& Proceedings of Indian Association for the Cultivation of Science)

ISSN 0973 - 1458

| | |
|---|---|
| **Periodicity** | 12 issues per year (January - December) |
| **Annual Subscription** | **(Per volume of 12 issues)** |
| (i) Foreign | US $ 550-00 (including Air-Mail Postage) |
| (ii) Inland | Rs. 2,000-00 (including postage) |
| **Single Issue** | |
| (i) Foreign | US $ 55-00 (including Air-Mail Postage) |
| (ii) Inland | Rs. 200-00 (including postage) |

*25% discount is allowed to Agents and Book-sellers.*

*50% discount is admissible to Research workers and Students for direct subscription.*

The annual subscription for **Members of IACS & IPS is Rs. 700.00** only, if the Subscription be received within 31st December, 2008 for Vol. 83 (2009).

**Demand Draft (D/D) should be drawn on any Bank of Kolkata Branch *in favour of***

***"Indian Association for the Cultivation of Science"***

Out-station cheque may be accepted with an additional amount of **Rs. 100-00**, in addition to Subscription Rates of **Rs. 2,000-00**

Journals and Reprints will be supplied against ***advance payment only.***

Phone : (+91) (33) 2473-4971 Extn. 160 Fax : (+91) (33) 2473-2805
e-mail : **ijp@iacs.res.in / ssahoo_ijp@yahoo.com**
Web : www.iacs.res.in/ijp.html

*Indian J. Phys.* **82** (**12**), 1751 (2008)

# INDIAN JOURNAL OF PHYSICS
## INDIAN ASSOCIATION FOR THE CULTIVATION OF SCIENCE
JADAVPUR, KOLKATA-700 032, INDIA

# Renewal / New Order Form
## Volume 83 (2009)

To : Mr. S. Sahoo,
The Assistant Registrar-I,
Indian Journal of Physics,
IACS, Jadavpur,
Kolkata-700 032, India.

- We would like to Renew our official order for the Indian Journal of Physics Volume 83 for the year 2009 (January to December).
- Our Subscription No. of 2008 is : _____
- We are placing our Official (**Renewal / New**) order for one year, i.e. 2009.
- Our purchase order No. is : _____ dated _____
- Please send your Proforma Invoice/Bill for 2009.
- Please acknowledge receipt of our order and/or advance payment.

Please despatch the journals at the following address :

Name :

Address:

Fax No.

Signature : E-mail Address :

Designation and official seal : Date :

*Indian J. Phys.* **82** (**12**), 1753 (2008)

# INDIAN JOURNAL OF PHYSICS
# INDIAN ASSOCIATION FOR THE CULTIVATION OF SCIENCE
# JADAVPUR, KOLKATA-700 032, INDIA

## SUBSCRIPTION RATES : VOLUME 83 (2009)

### INDIAN JOURNAL OF PHYSICS &
### Indian Association for the Cultivation of Science

ISSN 0973 - 1458

| | | |
|---|---|---|
| **Periodicity** | : | 12 issues per year (January - December) |
| **Annual Subscription** | : | **(Per volume of 12 issues)** |
| (i) Foreign | : | US $ 550-00 (including Air-Mail Postage) |
| (ii) Inland | : | Rs. 2,000-00 (including postage) |
| **Single Issue** | | |
| (i) Foreign | : | US $ 55-00 (including Air-Mail Postage) |
| (ii) Inland | : | Rs. 200-00 (including postage) |

*25% discount is allowed to Agents and Book-sellers.*

*50% discount is admissible to Research workers and Student for direct subscription.*

The annual subscription for **Members of IACS & IPS Is Rs. 700-00** only, if subscription be received within 31st December, 2008 for Vol. 83 (2009).

**Demand Draft (D/D) should be drawn on any Bank of Kolkata Branch**
***in favour of***

***"Indian Association for the Cultivation of Science"***

Out-station cheque may be accepted with an additional amount of **Rs. 100-00**, in addition to Subscription Rates of **Rs. 2,000-00**

Journals will be supplied against **advance payment only.**

---

Phone : (+91) (33) 2473-4971 Extn. 160 Fax : (+91) (33) 2473-2805
E-mail : ijp@iacs.res.in / ssahoo_ijp@yahoo.com
Web : www.iacs.res.in/ijp.html

Cover Designed by : IACS Drawing Office

Printed and Published by the Registrar, Indian Association for the Cultivation of Science, 2A & 2B, Raja Subodh Chandra Mallik Road, Kolkata 700 032, India at M/s. Print Home, 209A, Bidhan Sarani, Kolkata-700 006, India

Vol. 82, No. 12, December 2008
82 (12) 1609-1756 (2008)
REGISTERE
Postal Regn. No. SSRM/KOL RMS/WB/RNP-226/20
SSRM/KOL RMS/WB/RNP-226/FGN-30/2
RNI No.
ISSN

# INDIAN JOURNAL of PHYSICS

## CONTENTS



*[Cont'd. on 3rd cover]*